UNIVERSITY OF CALIFORNIA

SANTA CRUZ

DETECTING MELTWATER IN THE AMUNDSEN SEA POLYNYA REGION, WEST ANTARCTICA

A thesis submitted in partial satisfaction
of the requirements for the degree of

MASTER OF SCIENCE

in

OCEAN SCIENCES

by

Evan Randall-Goodwin

June 2012

The Thesis of Evan Randall-Goodwin
is approved:

_____
Assistant Adjunct Professor
Sharon Stammerjohn, Chair

_____
Professor A. Christina Ravelo

_____
Professor Andrew Moore

_____
Tyrus Miller
Vice Provost and Dean of Graduate Studies

Table of Contents

List of Figures

List of Tables

DETECTING MELTWATER IN THE AMUNDSEN SEA POLYNYA REGION, WEST ANTARCTICA

Evan Randall-Goodwin

Abstract

The Amundsen Sea Polynya International Research Expedition (ASPIRE) (Dec 2010 - Jan 2011) investigated high latitude (71-75S, 110-120W) ocean dynamics to better understand the polynya's high biological production. Hydrographic and dFe data from Conductivity-Temperature-Depth (CTD) measurements highlight a melt-laden outflow emanating from the Dotson Ice Shelf (DIS) and flowing between 400-600 m throughout the Dotson trough. Observations in the polynya near icebergs show water mass mixing of meltwater and Circumpolar Deep Water and elevated concentrations of dFe, indicating that drifting icebergs could deliver iron into the mixed layer either from in situ melt or by mixing up melt-laden outflow waters from the DIS. Time series data at the DIS outflow indicate warming since 2007. Although nearby Pine Island Glacier (PIG) outflow is overall warmer and saltier than DIS outflow, calculated meltwater fractions show similar relative quantities of meltwater from both PIG and DIS.

Acknowledgements

I would like to thank Sharon Stammerjohn, the most considerate, encouraging, generous and helpful adviser I could have hoped for. Sharon supported me throughout my entire masters degree and provided the right balance of guidance and freedom while researching this topic. I am always amazed how well Sharon can articulate and break down complex, scientific issues while teaching others. I am truly grateful to have worked with and learned from Sharon.

Thanks to the entire ASPIRE team for such an amazing first research cruise! I would especially like to thank Rob Sherrell at Rutgers University for providing all of the iron data for this thesis. Rob and I go back a long time and I had an awesome time sailing with him. Thanks to Anna Alderkamp for being a great mentor and friend on the cruise and conferences. Thanks to all of the other grad students on the cruise who were great friends and made a 50+ day cruise go by so quickly.

I really appreciated all of the computer and programming help from Ken Mankoff in the Earth Sciences department. Ken is a tech-wiz and always helped when I had any computer related questions. Ken generously taught me how to use and integrate data into Google Earth, which was a vital tool in completing my degree.

Thank you to the entire Ocean Sciences faculty and staff that made my graduate school experience complete. I would especially like to thank Andy Moore and Christina Ravelo for participating on my masters committee and providing feedback.

A giant thanks to the 5th floor penthouse (Jon, Wendy, Misty, Peter, Dondra, Matt, Kevin, Claire, Ralph, Heather, Leslie, Sherry, Shiloh). You all made coming up to campus so much fun! I never new exactly what to expect on a given day, but you all provided excellent distractions and so much entertaining conversation.

Thanks to all of my riding (Brett, Ralph), surfing (Jon, Fabian, Matt, Kyle) and climbing (Dondra, Misty, Nilo, Fabian, Ryan, Robin) buddies. I had so much fun hanging out with you all and look forward to spending more time with you after graduation!

Thanks to my 'west coast' family for being so inviting and supportive. Theresa, Dave and Joe have welcomed Carey and I into their house on so many holidays or random weekends. I am always glad to make the trip up to Sacramento and relax with such great people.

I'd like to thank my parents and siblings for coming out to visit me all the way from the east coast. Will and Emily both came out to visit a bunch of times on various school breaks and I always was excited to show them around Santa Cruz and explore more of California. My parents always supported my graduate career and I am very grateful for them providing me the opportunity to make it this far in my education.

Lastly, I want to thank Carey for everything over the past 6 years. I am so grateful for your constant encouragement and support and I enjoy all of the time I spend with you. Our trip to New Zealand after the cruise was unbelievable! And our hike through Abel Tasman is one of my favorite memories. I can't wait to spend more time with you and Thule!

1. Introduction

1.1. The ASPIRE project and objectives

The Amundsen Sea Polynya International Research Expedition (ASPIRE) occurred aboard the R/V Nathaniel B. Palmer between December 2010 – January 2011 to investigate why the Amundsen Sea Polynya (ASP) is on average the most productive (per m^2) polynya in Antarctica (Arrigo et al., 2003) (Figure 1). ASPIRE was a collaborative effort between multiple international teams including chemical, biological and physical oceanographers. The physical location of the ASP is remote (Figure 1, inset), and prior to this cruise there have been few shipboard measurements of the ASP region. One main hypothesis of ASPIRE was that nutrient-rich modified Circumpolar Deep water (mCDW) enters the ASP from the shelf break and fuels primary production. The presence of mCDW on the continental shelf has two significant ramifications: at the coast, it may be a heat source accelerating glacier melt (Jacobs et al., 2011) and thus enhancing the delivery of iron-laden meltwater to the ASP region, and it may alter water column stratification in the polynya, providing bioavailable iron through mixing and upwelling (Hiscock et al., 2003).

Water column structure and water mass interactions are poorly understood in the central Amundsen Sea. How mCDW enters onto the continental shelf and its return flow are equally vague. Wåhlin et al., (2010) describe the circulation of mCDW entering from the shelf break via submarine

troughs (Figure 1b), which lead to the underside of the Dotson Ice Shelf (DIS). It is then inferred that a geostrophically driven outflow returns a melt-laden water mass into the ASP where it is potentially entrained into the upper ocean by wind mixing and drifting icebergs. This melt-laden layer, originating at the DIS and other ice shelves east of the polynya (e.g., Pine Island Glacier, Thwaites), is a presumed iron source to the region. Drifting icebergs stir the water column, potentially upwelling melt-laden water into the upper mixed layer, which could fuel primary production.

Previous studies in the Amundsen Sea have not focused on the DIS outflow but acknowledged the potential for a geostrophically steered outflow of melt-laden water (Potter et al., 1988, Wåhlin et al., 2010). There is a paucity of historical data near the DIS and within the Dotson trough system. Our study attempts to determine the pathway(s) of mCDW entering the polynya, how it interacts with the DIS, and how the melt-laden outflow reaches the surface mixed layer to fuel primary productivity. We first examine the properties and spatial extent of (inflowing) CDW and (outflowing) melt-laden water in the vicinity of the Dotson trough and in the shallower Amundsen Sea plateau region to the east. We then characterize the melt-laden outflow using a meltwater fraction calculation and describe possible mechanisms of dispersion as it enters the polynya interior. We examine how drifting icebergs, which are ubiquitous in

the ASP region, can mix melt-laden water and mCDW (micronutrient rich and >2°C above the in situ freezing point) to mid-water column depths.

1.2. The Amundsen Sea Polynya

The Amundsen Sea Polynya is a naturally forming, perennially occurring area of open water surrounded by sea ice (Figure 1a). The ASP appears from November to March and is driven by latent heat transfer (Arrigo et al., 2003). Polynyas act as windows from the atmosphere to the ocean and permit the exchange of heat, solar radiation, and gasses between the ocean and atmosphere. Arrigo et al. (2003) studied 37 coastal Antarctic polynyas using remote sensing techniques and calculated that the ASP was the most seasonally productive (per m^2), with chlorophyll-a values reaching up to 2.2±3.0 mg/m^3. Despite its relatively small size (38,000 km^2), its annual production of 5.5±1.8 Tg C/yr was comparable to the larger (66,200 km^2) Prydz Bay Polynya in eastern Antarctica (Arrigo et al., 2003). Primary productivity is higher yet variable in the ASP, likely due to enhanced, but climate-sensitive sources of bioavailable iron.

The ASP, located between 73-74° S and 111-116° W in the central Amundsen Sea (Figure 1a) is bounded to the east by the Thwaites Ice Tongue, to the south by the Western Antarctic Ice Sheet (WAIS) and Marie Byrd Land (specifically the DIS between the Bear and Martin Peninsulas), and to the north and west by sea ice. The polynya occurs mostly over the shallow, broad continental shelf, but also extends over the deep Dotson trough, which bisects

the continental shelf on the western side of the ASP region (Figure 2). Thus, depths within the ASP range from <300 m to >800 m and the continental shelf extends ~263 km from coast to shelf break (Arrigo et al., 2003).

Another important question for ASPIRE was the possibility of polynyas acting as carbon sinks. Antarctic polynyas are typically associated with high net phytoplankton production and a short food chain, ideal for sequestering carbon to the deep ocean (Sarmiento et al., 1984). Antarctic waters tend to be co-limited by both iron and light, as there are sufficient macronutrients within the upper mixed layer (Arrigo et al., 1998). Iron is largely contributed by upwelled CDW, atmospheric deposition, sediment resuspension and/or glacial meltwater sources (Hiscock et al., 2003). Light is controlled by seasonal sea ice coverage, winds and clouds (Smith and Nelson, 1985).

1.2.1. A climatically changing environment

The WAIS is the southern boundary of the Amundsen Sea and is drained by fast moving ice streams including Pine Island Glacier (PIG) and the Thwaites Ice Tongue (Shepherd et al., 2001). The Amundsen Sea sector of the WAIS is the most rapidly changing area in terms of grounding line retreat and ice shelf thinning (e.g., Rignot et al., 2008) and together with the Bellingshausen Sea (to the east) has lost more sea ice than anywhere else in the Antarctic since the 1970's (Jacobs, 2006; Stammerjohn et al., 2012). As climate change brings significant changes to the physical environment in the Amundsen Sea, future

changes in community structure could be abrupt and drastic. For example, along the western Antarctic Peninsula (wAP), Montes-Hugo et al. (2009) noted that as poleward regions experience a warmer climatic shift, a coincident shift from a krill-based to a salp-based community might also occur. Warming could latitudinally shift upper trophic level predators to other Antarctic regions to feed on the krill.

In the Amundsen Sea region, sea ice extent and duration are rapidly changing. The combined Bellinghsausen-Amundsen Sea region experienced a 6% per decade reduction of sea ice coverage (Comiso and Nishio, 2008), as well as an earlier spring sea ice retreat by 31±10 days and a later autumn sea ice advance by 54±9 days over 1979-2006 (Stammerjohn et al., 2008). Current climatic changes allow more solar radiation to enter the polynya. Longer open-polynya seasons permit more wind mixing, altering stratification impacting total primary production. However, another impact of a longer polynya season is increased solar warming of the surface ocean and sea ice melting, which together create a shallow, warm, freshwater lens. This could lead to increased stratification and have profound effects on phytoplankton community structure, likely effecting carbon export fluxes.

1.2.2. Continental shelf bathymetry of the ASP

The present day Amundsen Sea continental shelf was shaped during previous glaciations, as the continental ice sheet, fed by tributaries from deeper

in the WAIS, advanced and retreated over the shelf (Nitsche et al., 2007; Walker et al., 2007). Previous advances of the WAIS during the last glacial maximum ~21,000 years ago (Conway, 1999; Turner et al., 2009) carved out troughs, creating the irregular and complex bathymetry of the Amundsen Sea. Currently, these deep troughs extend beneath the edges of the floating ice shelves, allowing warm mCDW access to the glacial grounding lines. Grounding lines are where the ice sheet is in contact with the seafloor and appear to be the first location to experience melting from mCDW (Nitsche et al., 2007; Jacobs et al., 2011).

In many regions of Antarctica, the continental shelf acts as a topographic barrier impeding access of warm CDW, which flows offshore from west to east within the Antarctic Circumpolar Current (ACC) (Figure 3). The bathymetry of the Amundsen Sea is unique in that it slopes downward towards the coast (Nitsche et al., 2007; Figure 3b). The troughs that bisect the continental shelf allow dense CDW (27.70 kg/m^3) to flow at depth towards the coast (Walker et al., 2007). Thus, these bathymetric troughs act as conduits for intrusions of mCDW to reach the ice shelf grounding lines (Nitsche et al., 2007; Walker et al. 2007).

The troughs in the eastern Amundsen Sea (~100-110° W) feed toward the eastern Bear peninsula and further on into Pine Island Bay. The central Amundsen Sea (~110-120° W), inclusive of the ASP region, contains one pronounced trough system, which extends from the continental shelf break and

splits towards the DIS and Eastern Getz ice shelves. The sill depths of the two troughs leading to the eastern Amundsen are each >600 m deep and allow relatively unmodified CDW to enter onto the eastern shelf (e.g., Walker et al., 2007). In contrast, the central Amundsen sill depth at the Dotson trough is only ~510 m deep, which may cause more modification of CDW at the shelf break by enhanced mixing with overlying winter water (WW) (Figure 3c). Distance between the shelf break and the southern meanders of the ACC also plays a role in how much CDW enters onto the shelf (Orsi et al., 1995; Martinson, 2011) and its degree of modification, as discussed in the next section.

1.2.3. Ocean circulation

The eastern limb of the Ross Gyre is situated offshore of the shelf break in the Amundsen Sea. Its actual location depends on seasonality, the location of the Amundsen Sea atmospheric low-pressure system (ASL), and other atmospheric forcing variability (as will be described in greater detail in the next section). The ACC travels from west to east along the northern section of the Ross Gyre. The southern boundary of the ACC, the source of Upper Circumpolar Deep Water (UCDW), reaches the continental margin in the eastern Amundsen Sea (Orsi et al., 1995). The ACC is made up of Lower Circumpolar Deep Water (LCDW; >1600 m), UCDW (<1600 m, >200 m) and surface waters with isopycnals shoaling toward the shelf break (Orsi et al., 1995).

As described above, the continental shelf break between ~100-120° W has three main trough systems, and these are deep enough to allow UCDW to spill into the inner continental shelf (Nitsche et al., 2007). The Dotson trough is primarily fed through a depression in the shelf break at -118° W, whereas PIG is fed by two converging trough systems originating at -113° W and -102° W (Figure 3a). Walker et al. (2007) describe how submarine troughs with deepening bathymetry towards the coast act as conduits for CDW to reach ice sheet grounding lines.

The distance between the shelf break and the southern meanders of the ACC primarily dictates how much CDW or mCDW enters onto the continental shelf (Orsi et al., 1995; Martinson, 2011). In the central Amundsen Sea region, the ACC exists ~130 km offshore of the Dotson trough. However, there are variable and complex current interactions between the ACC and the Ross Gyre, and it is believed that where the Ross Gyre and the ACC bifurcate there are weaker currents and a smaller onshore flow of CDW. Thus, the inflow of CDW at the Dotson trough is thought to be less than in the eastern Amundsen Sea where the ACC flows closer (~50 km) to the shelf break (Wåhlin et al., accepted). The diminished inflow of mCDW, coupled with the longer distance between the Dotson trough and the ACC, allows for a higher degree of modification of CDW entering the central Amundsen Sea region. Thusly, compared to mCDW entering

the eastern Amundsen Sea region, mCDW in the central Amundsen Sea region is cooler and fresher (Wåhlin et al., accepted; Yuan et al., submitted).

Consequently, the eastern and central Amundsen Sea regions have distinct water mass properties. The eastern Amundsen is warmer and saltier below the pycnocline than the central Amundsen, from minimally-modified CDW entering into the Pine Island Bay trough system (Jacobs et al., 1996; Wåhlin et al., accepted; Yuan et al., submitted). On average waters below the pycnocline in the central Amundsen are ~0.70°C cooler and 0.15 psu fresher than the eastern Amundsen (Yuan et al., submitted). A ridge like bathymetry (the Amundsen Sea plateau, -110° W) extending from the Bear peninsula to the continental shelf break rises as shallow as 300 m and may largely prevent lateral mixing between the two basins. The stark difference in water mass properties is a result of multiple factors, including proximity to the ACC at the shelf break and the shelf break sill depth discussed above.

In the Dotson trough, the inferred circulation suggests that warm, salty mCDW flows south at depth along the eastern bank of the trough leading to the DIS (Nitsche et al., 2007; Wåhlin et al., 2010). Upon reaching the coast, mCDW flows under the DIS, becomes entrained with basal meltwater and then exits the ice shelf as buoyant mixture of meltwater and mCDW. An unknown amount of this melt-laden mixture flows northward along the western bank of the trough in a broad, slow moving layer (Wåhlin et al., 2010). Preliminary estimates suggest

that the Dotson trough system allows between 0.3 to 0.4 Sv of CDW to flow towards the continent (Wåhlin et al., 2010).

In general, meltwater appears to be more prevalent in the central Amundsen than in the eastern Amundsen (Wåhlin et al. 2010; Yuan et al., submitted), perhaps enhanced by a theorized coastal current flowing from the eastern basin into the central basin, delivering large quantities of melt-laden water. Thus, the water in the central basin is also not as strongly stratified as the eastern basin due to more highly modified (cooled and freshened) CDW at depth. Weaker stratification may encourage more vertical mixing between WW and a melt-laden layer of ice sheet origin (Yuan et al., submitted).

1.2.4. Atmospheric Circulation

Largely driven by atmospheric forcing, mCDW from UCDW origin, selectively enters onto the Amundsen Sea continental shelf at depressions in the shelf break as described above (Orsi et al., 1995; Walker et al., 2007). The Amundsen Sea Low (ASL) is the dominant atmospheric pattern found in the Amundsen Sea region and seasonally migrates from offshore of the shelf break at ~100° W (in summer and early fall) towards the continental shelf at ~140° W (in late winter and early spring) (Thoma et al., 2008). The ASL, like all low-pressure systems in the southern hemisphere, spins clockwise. In summer, with the ASL north of the shelf break, the dominant winds at the shelf break are easterly and southerly winds. The ASL diverts the northern limb of the Ross

Gyre to the west and north, which shifts the ACC further away from the shelf break, limiting influx of CDW onto the continental shelf. According to Thoma et al. (2008), in late winter to early spring the ASL shifts to the south and west, causing the dominant winds near the shelf break to be westerly and northerly (see also Steig et al., 2012). Thus, winter-spring conditions encourage the northern limb of the Ross Gyre to shift toward the south, allowing the ACC to flow along the shelf break, enhancing CDW penetration onto the continental shelf (Thoma et al., 2008).

When westerly winds at the Amundsen Sea shelf break do prevail, they cause "northward Ekman transport of surface waters, which drive an eastward geostrophic current and an associated upslope, on-shelf flow of mCDW within the bottom boundary layer" (Steig et al., 2012). Further, studies indicate a positive teleconnection between central tropical Pacific SST and westerly winds near the Amundsen Sea (Ding et al., 2011; Schneider et al., 2012; Steig et al., 2012). Between 1980-89 and 1990-99 SST's in the tropical Pacific increased on average by 0.3°C. Concurrently, since the 1990's, westerly winds have increased along the Amundsen Sea shelf break, presumably driving more mCDW onto the Amundsen Sea embayment (Thoma et al., 2008; Jacobs et al., 2011; Steig et al. 2012).

Additionally, annual longitudinal migration of the ASL is variable and affected by atmospheric phenomena including the Southern Annular Mode

(SAM) and El Nino Southern Oscillation (ENSO) (Stammerjohn et al., 2008; Schneider et al., 2012). Therefore, interannual variability of CDW entering onto the continental shelf can be significant and it is inferred that with strengthening northerly and westerly winds, more CDW will enter onto the continental shelf (Thoma et al., 2008). During positive phases of the Southern Annular Mode (SAM), or a strong La Nina, the Amundsen Sea Low strengthens poleward, shifting the ACC closer to the shelf break in the eastern-central Amundsen Sea and causing an increase in north-westerly winds. This could periodically bring more mCDW onto the continental shelf. Several studies (e.g., Marshall, 2003; Stammerjohn et al., 2008) have indicated a trend towards more positive SAM conditions, which could potentially increase the transport of CDW across the shelf break.

1.2.5. Meltwater from glaciers

As described above, the trough system leading to PIG is a combination of two entrance sills at the eastern Amundsen continental shelf break, which converge on the continental shelf and extend under PIG. The general circulation in the Pine Island Bay trough system consists of warm mCDW flowing along the trough from the continental shelf break to the underside of PIG. The mCDW melts the bottom of the ice shelf near the grounding line, becomes more buoyant by mixing with fresh meltwater and exits as a geostrophically driven outflow (Potter et al., 1988; Jacobs et al., 2011).

The outflow from under PIG has a relatively large fraction of meltwater which can be quantified at >15 ppt in the upper water column (Jacobs et al., 2011). The fate of the outflow is unknown, although it is inferred to flow to the west as part of a coastal current (Jacobs et al., 2002). A recent study shows stronger circulation of mCDW under PIG and an associated increase of melting and thinning of PIG (Jacobs et al., 2011). However, mCDW measured after it interacted with PIG was on average only 0.5°C cooler than when it entered, indicating that not all of its heat was lost to melting ice (Jacobs et al., 2011).

Many of the ice shelves of the WAIS, especially PIG, are currently experiencing high basal melt rates, which cause ice shelf thinning and accelerated glacier flow upstream (Nitsche et al., 2007; Jacobs et al., 2011). When mCDW encounters the underside of the floating ice shelf, it encourages melting through latent heat transfer and water mass modification through cooling and freshening (Jacobs, 2006; Wåhlin et al., 2010). The DIS has a relatively slow velocity of 0.2-0.5 km a^{-1} (Rosanova et al., 1998) and is thinning at ~10 cm a^{-1} (Rignot et al., 2008). In comparison, PIG is retreating from its grounding line at 1.2 km a^{-1} (Rignot, 1998) and is thinning at 1.6 m a^{-1} (Shepherd et al., 2001). The extreme difference in ice shelf retreat might be attributed to less-modified (i.e. warmer) mCDW entering into the Pine Island Bay trough system, causing more rapid melting and thinning of PIG.

Our study site was at the DIS, which is ~50 km wide and faces northward between the Martin and Bear Peninsulas. The DIS originates from the land based Kohler and Horral Glaciers, which branch off of the larger Smith Glacier (Lucchitta et al., 1994). The DIS is a dynamic ice shelf characterized by notches, protruding sections and frequent collapses (~10 m^3). The bathymetry in front of the DIS features the Dotson trough, which is deepest in the center and shallows slightly to the east and more strongly to the west along the ice shelf front.

1.2.6. Meltwater from icebergs

Glacial meltwater is enriched with iron and other micronutrients from glacial scouring of crustal material and includes also a small amount of aeolian deposition (De Baar et al., 1995). Meltwater from both ice shelf and iceberg melt is thus enriched in micronutrients. When an iceberg breaks off of a glacier, it becomes a source for micronutrients and terrigenous sediment (Neshyba, 1977; Smith et al., 2007). Previous studies (e.g., Dierssen et al., 2002) do not indicate that elevated macronutrients (i.e. silicate and phosphate) are associated with coastal, glacial melt water inputs; rather macronutrients are upwelled from deeper waters. Icebergs typically follow well-defined courses dictated by local winds and currents. Along their drift paths, icebergs redistribute heat, fresh water, macronutrients by mechanically mixing the water column and micronutrients (iron) from in situ melting or mixing (Jenkins, 1999; Smith et al., 2007; Stephenson Jr. et al., 2010). In the close vicinity of a free drifting iceberg

there can be an increased concentration of iron and chlorophyll (Smith et al., 2007) with up to a 1/3 increase of phytoplankton biomass in its wake (Schwarz and Schodlok, 2009).

Waters directly surrounding an iceberg are therefore associated with distinct chemical characteristics and biological activity, including the presence of higher trophic level predators such as birds and seals (Smith et al., 2007). As a wind-driven iceberg drifts through the ocean, its keel mechanically stirs up the water column; the associated melting and mixing cause upwelling of waters rich in iron, nitrate, phosphate and silicate (Hiscock et al., 2003; Schwarz and Schodlok, 2009). For medium sized (order 1 km^2) icebergs, the bottom topography and keel depth (often reaching 140-600 m deep), as well as drift velocity and ocean current velocity, often determine the intensity of water mass mixing (Schwarz and Schodlok, 2009). When exposed to the correct conditions, the upwelling of nutrient-rich deep waters, along with the release of micronutrients by basal iceberg melting, can have positive impacts on phytoplankton growth.

Our iceberg study site was at 113.6° W, 73.7° S and consisted of a free floating, 3 km x 1 km iceberg with an irregular freeboard ranging from 37-50 m and an estimated keel depth ranging from 340-450 m. The iceberg height was measured by sextant and was used to calculate iceberg keel depth using isostatic principles. The study location was approximately 30 km north of the DIS

outflow region, within the ~700 m isobaths of the Dotson trough. Previous studies in the Weddell Sea have shown that the thermocline is altered by the turbulent entrainment of meltwater at the base of drifting icebergs (Stephenson Jr. et al., 2010). Several CTD casts were taken near the iceberg, both down- and upstream of its drift trajectory (and prevailing ocean currents), to determine the degree of mixing and melt-laden water associated with the iceberg's drift. These results will be presented below in Section 3.

2. Data and Methods

ASPIRE occurred December 2010 - January 2011 aboard the RV/IB Nathaniel B. Palmer (cruise number NBP1005) and conducted hydrographic, biological and biogeochemical surveys of the ASP region. The cruise track strategically crossed bathymetric gradients and included a high-resolution survey along the DIS (Figure 1b). The hydrographic data comprised 87 conventional Conductivity-Temperature-Depth (CTD) casts, 35 Trace Metal Clean (TMC) CTD casts, and 92 Expendable Bathythermograph (XBT) profiles. The CTD package was a Sea-Bird Electronics, Inc., SBE 9/11+ system on a 24-bottle SBE32 rosette, equipped with dual temperature, conductivity and oxygen sensors. A single pressure sensor, rated to 6,000 dbar, provided pressure information for conversion to depth. Additionally, a single chlorophyll fluorometer, a transmissometer, and a PAR sensor were attached to the rosette.

CTD casts on the continental shelf typically reached within 10 m of the bottom, detected with a Benthos PSA-916 altimeter and a SBE bottom contact with a 10 m line. The TMC package was new for this cruise and was equipped with a similar suite of Sea-Bird Electronics sensors as the conventional CTD. The sensors on both CTD's were calibrated before and after the cruise, and the data were processed post cruise to correct for drift in temperature and salinity measurements. Onboard, the salinity and oxygen sensor data were spot-checked against discrete samples using an Autosal and the Langdon Oxygen titrator.

Ocean currents were measured with a Teledyne RD Instruments, Inc 'narrow beam' 150-kHz (nb150) and 'Ocean Surveyor' 38-kHz (os38) hull mounted Acoustic Doppler Current Profilers (ADCP). The ADCP data were calibrated and post cruise corrected by Eric Firing and Jules Hummon at University of Hawaii. The nb150 data are accurate to 400 m, while the os38 has a larger depth range but coarser resolution. The ADCP data were not de-tided.

The nutrient data were collected on select CTD casts from Niskin bottle samples and analyzed each day using a flow injection analysis on a Lachat Instruments Quickchem 8000 Autoanalyzer. Kuria Ndungu and Maria Lagerstrom analyzed dFe data with a flow-injection Fe analyzer in the clean "bubble" aboard the NBP.

The Polar Geospatial Center at University of Minnesota and the National Snow and Ice Data Center (NSIDC) provided visible, infrared and microwave satellite data. The image data used in this study are from the MODIS (Moderate Resolution Imaging Spectroradiometer) 250 m-resolution instrument on the NASA Terra and Aqua satellites. Those data, when cloud-free conditions existed, provided excellent sea ice coverage, polynya boundaries, and spatial distribution of icebergs within the polynya.

DIS draft and bathymetry data were collected and processed by Kathleen Gavahan (Raytheon Polar Services Company) using the Simrad EM12 Multibeam aboard the NBP. On December 17 from 0900-1400 GMT the NBP performed a

transect dubbed the 'Iron Curtain"; the ship maintained a constant ~0.3 km distance from the ice shelf to record the approximate draft of the DIS, corresponding bathymetry and deploy XBTs every 2-4 km to obtain a cross section view of water temperatures. Meanwhile the underway measurements recorded surface properties, ocean currents, bottom depths and ice shelf draft. We also made 4 TMC and 1 CTD deployments at select locations of interest.

2.1. The Gade Line

Typical summer water column conditions at the DIS and PIG consist of mCDW at depth, which underlies (to varying degrees) a mixture of mCDW and glacial meltwater and/or surface waters (Jacobs et al., 2011). In summer, Antarctic Surface Water (AASW) is essentially Winter Water (WW) modified to varying degrees by seasonal sea ice melt and solar ocean warming. In winter WW is produced from sea ice production, which causes brine rejection, which in turn increases salinity and deepens the seasonal mixed layer (Orsi et al., 2009). (See Section 3.1 for further detail.)

When plotted in Temperature-Salinity (T-S) space, certain CTD data lie close to the prescribed mixing line between mCDW and glacier meltwater (Figure 4a), the so-called Gade line (Gade, 1979; Wåhlin et al., 2010). The Gade line is a theoretically derived equation, which when plotted in T-S space represents points where a mixture of CDW and glacial melt water exist. The Gade line thus provides a convenient visual reference for detecting meltwater

presence and is included on our T-S plots. Typical Gade line slopes for Amundsen Sea conditions range from 2.5 to 2.7 °C/psu with a zero salinity intercept at a prescribed continental ice temperature ranging from -50°C to -92.5°C (Gade, 1979; Potter et al., 1988; Jenkins, 1999). Data that deviate from the Gade line indicate less to no meltwater presence and more direct mixing between WW and mCDW (see Figure 4a).

2.2. Calculated Meltwater Fractions

Jenkins (1999) provides a series of equations to calculate the meltwater content at depths below the wind-mixed surface layer, based on ambient CDW and WW conditions of the region. Meltwater fractions (MWF) are calculated using the following generic equation:

$$\psi^{2,1} = (\chi^2 - \chi^2_{CDW}) - (\chi^1 - \chi^1_{CDW}) * (\chi^2_{WW} - \chi^2_{CDW}) / (\chi^1_{WW} - \chi^1_{CDW}) \quad (1)$$

The superscripts ^{1} and ^{2} represent conservative tracers for each specific water mass (i.e. temperature, salinity, O_2, $\delta^{18}O$). The fraction term on the right represents the observed properties (e.g., temperature and salinity) at depth in relation to the ambient CDW and WW properties. Assuming the composite tracer is a non-zero (a completely homogenous water column), the meltwater fraction is calculated by

$$\varphi = \psi^{2,1}_{mix} / \psi^{2,1}_{melt} \quad (2)$$

The denominator for equation (2) is the composite for pure melt water (Jacobs et al., 2011). When calculating melt water fractions using temperature and salinity data, we set T_{melt}=-92.5 °C and S_{melt}=0 psu based on fresh water in glaciers. The internal ice temperature is derived by extending the mixing line in T-S space to 0 psu (Jenkins, 1999; Jacobs et al., 2011). Other tracers include O_2 and $\delta^{18}O$, however our study, like Jacobs et al. (2011), used temperature and salinity data (Table 1).

For this study we use the following modified equations to derive meltwater fractions, where T_{Data} and S_{Data} represent the temperature and salinity profiles respectively:

$$ambientTS = (T_{WW} - T_{CDW})/(S_{WW} - S_{CDW}) \quad (3)$$

$$TS_{melt} = (T_{melt} - T_{CDW}) - (S_{melt} - S_{CDW})*ambientTS \quad (4)$$

$$TS_{mix} = (T_{Data} - T_{CDW}) - (S_{Data} - S_{CDW})*ambientTS \quad (5)$$

$$MWF = TS_{mix}/TS_{melt} \quad (6)$$

Equation (6) provides the calculated MWF and shows how much of the water column at a given depth is comprised of melt-laden water. Ambient values for WW and CDW are usually well-defined in T-S space; when this was not the case (e.g., in dynamically mixed waters near icebergs or in heavily melt-laden waters near DIS outflow), then ambient WW and CDW values from nearby (undisturbed) CTD profiles were used instead. MWF's provide an apt description of the water column in a multi-layer system when the tracers are

conservative (Jenkins et al., 2008). However, in the upper 0-100 m, the tracers are not conservative due to surface forcing by atmospheric processes, so we discount calculated MWF's above ~100 m.

2.3. Historical Data and Data Visualization

Two previous R/V NBP cruises to the Amundsen Sea (NBP0702 and NBP0901), led by chief scientist Stan Jacobs, provide some earlier observations of the DIS and ASP region. Both cruises included ample CTD stations across PIG and DIS, and during NBP1005 we intentionally repeated the DIS stations to facilitate temporal comparisons. These previous data were compiled, integrated, and analyzed using Matlab and Ocean Data View (ODV, http://odv.awi.de). For geo-locating and visualizing the space/time hydrographic data series, Google Earth (GE) was used. The GE "time slider" function allows for a 4th dimension of data and nicely shows the progression of data along the cruise track. Google Earth is an incredible tool for presenting ocean data, especially for toggling through multiple layers of time dependent data.

3. Results

3.1. Water mass types in the ASP region

In winter, there are two primary water masses in the ASP region: mCDW and WW (Figure 4a; Table 2). Originating from CDW offshore at depths ranging between 500-1500 m within the ACC (Orsi et al., 1995), mCDW on the shelf is

relatively warm, salty, oxygen-poor, and nutrient-rich. Relative to WW and AASW, mCDW has low oxygen due to depletion by respiration and its isolation from surface processes (e.g., atmospheric gas exchange; Figure 4b). In the trough regions, mCDW was found at depths >700 m and is the primary heat source in the ASP region. In contrast, over the Amundsen Sea plateau, east of the Dotson trough (at depths ranging from ~250-350 m), mCDW is more modified: cooler, fresher, less nutrient-rich than mCDW found in the deeper trough regions.

In winter, the water mass overlying mCDW is WW; a cold, fresh, oxygen-rich water mass, typically occupying the upper ~300 m. WW is formed by sea ice production and its temperature is usually at or near the in situ freezing point. In spring, sea ice melt creates AASW; a fresh, shallow, seasonal mixed layer that then warms with increased insolation. Thus, AASW is a warmed, freshened version of WW, with broad temperature and salinity ranges, reflecting different degrees of surface warming and meltwater inputs. In summer, beneath AASW is often a 'remnant' layer of WW, with thickness and modification reflecting the degree of vertical mixing with AASW from above and with mCDW from below. Subsequently, in autumn, when AASW cools to the freezing point, sea ice production commences. The brine rejection from sea ice production salinizes the freshwater layer, essentially reverting AASW back to WW.

Of particular interest are melt-laden layers detected at depth in the ASP region, most of which likely emanate from the DIS (and from other ice shelf

outflows) and extend to the continental shelf break. These layers were best identified using calculated MWF's and in temperature-salinity space in relation to the mixing line between CDW and pure meltwater (Figure 4a) following Gade (1979) and Wåhlin et al. (2010). Thus, during NBP1005, typical water masses or features within the Dotson trough consisted of the following (from surface to bottom): AASW, WW, a meltwater layer, mCDW (e.g., Figure 4b). In contrast, in some of the shallower regions east of the Dotson trough, the water column appeared only to consist of AASW and WW.

3.2. Underway Sea Surface Observations

Observations from underway sea surface measurements, specifically sea surface temperature (SST) and sea surface salinity (SSS), provide spatial and seasonal overviews of the ASP region (Figures 5 and 6). The NBP entered through dense patches of sea ice (not yet melting) in the western ASP on December 14, 2010 and observed cold (-1.8°C) and relatively salty (33.9 psu) surface values (which would turn out to be the coldest and saltiest surface values observed along the cruise track). Here, WW was still present at the surface and extended down to 300 m. On average, as seasonal winds and solar ocean warming remove sea ice within the ASP region, the surface area of the ASP grows to ~27,000 km^2 over ~73-74° S and ~110-120° W (based on satellite derived spatial coverage, averaged between 1997-2010) (Arrigo et al., 2012).

When the NBP exited the ASP on January 6, 2011, there was a 4°C increase in air temperature, >2°C increase in SST and 0.5 psu decrease in SSS as a result of the progression from austral spring to summer.

The warmest temperatures recorded in the interior polynya had been ice-free the longest and thus warmed the longest by solar insolation, with SST decreasing towards the sea ice-rimmed polynya (Figure 5). In general SSS will be lower where sea ice is melting, but the longer the waters are ice-free, the more they are exposed to wind-mixing. Winds mix down the shallow melt layer, which increases the surface salinity. Thus, SSS was higher in the middle of the polynya (which had been ice-free longer) and lowest where sea ice was actively melting, e.g., on the northward track leaving the polynya (Jan 6 onward) (Figure 6). Towards the end of the cruise a massive phaeocystis bloom reaching chlorophyll-a >45 mg/m^3 occurred over the Amundsen plateau (Figure 1a).

The NBP entered and exited through sea ice in the northwest corner of the ASP. As shown on the station map (Figure 1b), Station 4 was located near the continental shelf break, which was in the sea ice surrounding the polynya (Figure 1a). A CTD cast taken at that location showed a ~300 m deep mixed layer of WW overlying warmer, saltier mCDW. There was also some indication of a melt-laden layer between 300-400 m, i.e. below the WW but above the mCDW. (Melt layers will be discussed in greater detail in Section 3.6.). Station 4

was in the general vicinity of where mCDW would enter the shelf break via the Dotson trough.

Near the end of our research cruise, we held another station in the vicinity of Station 4, Station 68, which was slightly further offshore (of the shelf break) and in deeper water. The maximum temperature (Tmax) in the mCDW layer recorded at Station 68 was 1.2°C at 500 m, while at the shallower Station 4, Tmax was 0.8°C at ~600 m. Although Station 68 was only 13 km from Station 4, it was 150 m deeper and had access to less-modified CDW. In comparing Tmax at these two stations, it suggests CDW may be considerably modified as it enters the Dotson trough system.

By January 6, 2011, summer conditions prevailed and the northern sea ice boundary of the ASP was receding equatorward. Surface temperatures at Station 68 did not warm up quite as much as the polynya interior, but air temperatures and SST increased > 4°C and 0.5°C, respectively. Receding sea ice allowed the surface ocean to absorb incoming solar radiation, heating and stratifying the upper water column. Where sea ice was melting at the northern boundary of the ASP, SSS decreased from 34.9 to 34.3 psu (Figure 6). Over 27 days, the ASP shelf break developed a defined summer mixed layer in the upper 50 m. Surface stratification at the continental shelf break permitted significant phytoplankton growth with chlorophyll-a values > 1 mg/m^3. These chlorophyll-

a values are low compared to the polynya interior, but are high compared to the neighboring ACC (Boyd et al., 2000).

3.3. Cross sectional views of currents and water masses in the ASP region

As seen in Figure 1b, the cruise track at times followed or crossed the Dotson trough. Here we show a few examples of how water column properties (ocean currents, temperature, and salinity) varied along sections of the cruise track that either followed the trough or crossed it at various points. We note that the ocean currents shown in Figures 7-9, are from continuous underway ADCP observations (so continuous in time), whereas the temperature and salinity cross sectional plots are from all CTD observations in the vicinity of that transect. Therefore, the latter are not necessarily continuous in time due to the cruise track crisscrossing the ASP several times, thus offering repeated observations of the trough region in particular.

3.3.1. Along the Dotson Trough

A north to south transect along the Dotson trough (Figure 7) shows how water column properties varied from off-to-onshore, in particularly showing the variability in WW and mCDW layer thickness and modification. This particular transect started at Station 6 (Figure 1b), which occurred in the middle of the Dotson trough near the fork leading to the Getz Ice Shelf. It then continued southward to Station 8, near the central portion of the DIS (Figure 7e). Within

the trough region, WW (<300 m, -1.8°C) was overlying mCDW, which stayed near the sea floor (~700 m). At -73.8° S, -113.5 ° W, the water column showed strong mixing between WW and mCDW, which happened to be an area where an iceberg was drifting, and will be discussed in detail in Section 3.5.

The NBP then crossed the trough to the south and west and recorded northward currents along the western side of the trough near the Martin Peninsula. The western side of the Dotson trough was where we noted a northward flowing melt-laden layer that appeared to originate at the western DIS between 200-400 m (see Section 3.4). In contrast, Station 8 was east of the outflow region and exhibited WW overlaying mCDW and southward ADCP velocities,. In general, the southward velocities to the east in front of DIS, versus the northward velocities to the west, are qualitatively consistent with the inferred circulation in the Dotson trough region described previously in Section 1.2.3.

3.3.2. Across the Dotson Trough, Southern Transect

We next show an east to west transect across the Dotson trough, which begins at the eastern sea ice edge of the polynya, crossed the Dotson trough and finished over shoaling bathymetry north of the Martin Peninsula (Figure 8). The eastern portion of the ASP (-110° W to -112° W) lies over the shallow (<400 m) Amundsen Sea plateau region. The transect over this shallow plateau area was dominated by WW overlying a thin, highly modified CDW layer that appeared

cooler and fresher than the mCDW observed further west (i.e., in the deeper Dotson trough region). Alternating northward and southward currents across the Dotson trough could be indicative of tidal influences or potential eddy activity. However, the southward flow along the eastern side of the Dotson trough (-113° W) versus the northward flow along the western side of the Dotson trough (-114° W) is again consistent with previous observations. For example, using LADCP data, Wåhlin et al. (2010) noted that the west bank of the Dotson trough showed a diffuse northward flow, while southward flow was distinct along the east bank of the trough.

The central trough region exhibited an uplifted thermocline and halocline observed in the vicinity of an iceberg (which again will be discussed further in Section 3.5). Furthest to the west, on the Getz Ice Shelf side of the Martin Peninsula were southward currents, possibly indicating the continuation of a westward flowing coastal current, here diverted north then south around Martin Peninsula (Jacobs et al., 2002; Jacobs et al., 2011).

3.3.3. Across the Dotson Trough, Northern Transect

Roughly 50 km north of the Martin Peninsula, the NBP made another east to west transect across the Dotson trough, ending where the trough splits towards the Getz Ice Shelf (Figure 9). Bottom depths in the center of the trough were >1000 m with gradual shoaling to the east. As shown in the previous cross-trough transect that was further to the south (Figure 8), the ADCP currents

again indicate southward flow along the central and eastern portion of the Dotson trough. Without the drifting iceberg influence, we note more typical homogeneous water mass layers of WW overlying mCDW. This transect also crossed onto the Amundsen Sea plateau (to the east), but here it is less shallow with warmer, less-modified CDW at depth (as compared to the more modified CDW in the shallower plateau region to the south, Figure 8). It may also be that the northern cross-trough transect showed warmer mCDW at depth because of its proximity to the shelf break and source of CDW.

This transect was characterized by high biological activity measured at the surface. We recorded chlorophyll-a values >15 mg/m^3 in the trough and >30 mg/m^3 over the Amundsen Sea plateau (e.g., Fig 1a). High primary productivity was accompanied by low surface CO_2 concentrations (<170 ppm) and high surface oxygen (10.8 ml/L), likely enhanced by biological drawdown and production, respectively.

The ADCP transects described above are now viewed within the context of all the underway ADCP observations (Figure 10). Here, the currents were depth-averaged to show current structure with respect to sea floor bathymetry. Overall, the ASP had weak, variable currents and the only distinct feature was the DIS outflow (averaging >20 cm/s). Within the ASP, tidal currents < 3 cm/s are typical (Wåhlin et al., 2010). Our ADCP data have not been de-tided, so much of the low magnitude variability will likely be due to tides. We also note

some tidally enhanced currents in the center of the trough at -115° W, -73° S, and at -114° W, -73.5° S (north of the Martin Peninsula) where the cruise track crossed itself. At these locations we saw similar magnitude currents with varying directions, possibly indicating an ebb and flow of tides through the Dotson trough. However, the DIS outflow is the most distinct and strongly focused current in the ASP, narrowly concentrated on the western side of the ice shelf and consistent with the inferred sub-ice shelf circulation (e.g. Potter et al., 1988; Jacobs et al., 2011)

3.4. The Dotson Ice Shelf Study

The NBP conducted a CTD, XBT and underway ADCP survey in front of the DIS dubbed the 'Iron Curtain'. While steaming from east to west at ~0.3 km from the ice shelf front, we deployed 17 XBT's (every 2 to 4 km). The 'Iron Curtain' transect allowed us to obtain a high resolution cross sectional map of temperature and currents in front of the DIS. Four TMC and one CTD casts anchored the survey and were used to help verify XBT data, and in the case of the former, provide invaluable measures of trace metal properties. Our findings are described below in 3.4.1.

Sub-ice shelf processes are quite complex and generally unobserved; we therefore use basic Coriolis and geostrophic principles to make generalizations on water mass flow and mixing. Figure 11 provides a conceptual view of the inferred circulation under the DIS. As warm, salty mCDW circulated under the

DIS along the eastern part of the Dotson trough, it was freshened and cooled by basal ice shelf melt and contributed to an outflow current along the western boundary. Coriolis inflow should be concentrated on the eastern side of the sub-ice shelf cavity, while outflow would be on the western side. However, this does not mean that inflow is not happening everywhere at depth, but likely not as concentrated as on the eastern side, and similarly, outflow may be happening everywhere at mid-depths and may be influenced/directed by sub-ice shelf topography (e.g., Bindschadler et al., 2011; Mankoff et al., 2012).

3.4.1. DIS Cross Sectional Views of Currents and Temperature

In front of most of the DIS, north-south currents were variable and relatively weak. However, a distinct inflow (southward) current was observed at the far eastern boundary, particularly at depths below 500 m, while a distinct (northward) outflow current was observed at the far western boundary and was considerably shallower and stronger (>0.25 m/s) between ~150-350 m (Figure 12). The top 50 m and the 100 m above the bottom contain noisy data ADCP and were therefore excluded. However, the inflow is inferred to continue at depth on the eastern side of the Dotson trough, and although it is not entirely captured by the ADCP data, it is confirmed by non-melt-laden mCDW as will be shown in Figures 13 and 15. The ADCP current data from this transect is from December 17, 2010 09:12-14:12 and has not been detided. Banded north/south currents

between the enhanced eastern inflow and western outflow could represent channelized flow associated with ice shelf basal channels (Mankoff et al., 2012).

The temperature transect across the DIS (Figure 13a) featured a shoaling thermocline to the west. Correspondingly, we note that the DIS draft was ~100 m thinner on the western side than in the east. The -0.5°C isotherm typically appeared at ~350 m but shoaled to ~250 m between -113.1° W to -113.4° W longitude. The tilted thermocline was associated with the strong outflow described above (Figure 12) and a distinct melt-laden layer (discussed in detail in the next section). The temperature of the outflow waters were ~1°C warmer than the in-situ freezing point. The five CTD profiles taken along the 'Iron Curtain' transect extended observations to the full seafloor depth (and served as quality-control of the XBT data). The CTD data show mCDW (>0.4°C; >600 m) prevalent at depth.

For comparison, the DIS outflow waters were cooler and fresher (> -0.5°C, 33.76 psu) than mCDW at depth, but warmer and saltier than WW (< -1.4°C, 33.84 psu) observed in the 150-300 m depth range east of the outflow region. When plotted in T-S space (Figure 13b), it becomes clear that the water properties in the DIS outflow (as captured by the TMC29 cast) are distinctly different than at the other CTD stations. Data from the DIS outflow lies close to the mixing line between mCDW and meltwater (discussed in greater detail in the next section).

A DIS temperature anomaly plot (Figure 14) was created by subtracting the mean temperature at a given depth observed along the DIS front from the same depth at each CTD/XBT (using data shown in Figure 13). Positive 0.7°C anomalies occurred between 200-400 m at the western boundary of the DIS and corresponded to the strong outflow centered at -113.33° W. However, it is noted that the strongest temperature anomalies were ~150 m below the ice shelf draft (which, as noted above, was relatively thin at ~150 m). This apparent 'buffer' zone prevented the warmest outflow waters from directly contacting the DIS, at least as observed directly at the ice shelf front.

3.4.2. Calculated Meltwater Fractions in Front of the DIS

We calculated melt water fractions (MWF's) at five stations across the DIS following the work of Jenkins (1999) and Jacobs et al. (2011). Low MWF values were observed at depths >600 m, where mCDW was observed in CTD profiles in the eastern trough (TMC9, TMC11, CTD7) (Figure 15). MWF's were also low between ~200-300 m where WW was detected in the CTD profiles east of the strong outflow region. At the DIS outflow (TMC29) between 200-400 m, we saw MWF's >15 ppt, comparable to MWF's observed in the outflow waters of Pine Island Glacier (PIG) (Jacobs et al., 2011). MWF's were highest between ~200-300 m at the DIS outflow, the same location where the most positive temperature anomalies were observed.

The CTD profiles in front of the DIS also exhibited low surface dissolved oxygen values compared to the central ASP, indicating a presence of oxygen poor mCDW appearing in the mixed layer. Low chlorophyll-a values along the DIS were also noted with the underway fluorometer data (e.g., Figure 1a), potentially because phytoplankton did not have time to bloom before being advected into the polynya (Alderkamp et al., in press) and/or because the mixed layer was too deep (Figure 13).

DIS outflow was enriched with dFe compared to the interior polynya (Figure 16). Enrichment could be from sediment resuspension near the grounding line or from basal ice shelf melt (Planquette et al., 2011). As discussed in the Introduction, iron is considered the limiting micronutrient in the ASP (Boyd et al., 2000; A. Alderkamp, Stanford University, pers. comm.). Elevated dFe at the DIS outflow and at specific depths throughout the Dotson trough appear to indicate the presence of a melt-laden water mass. This will be investigated and discussed in greater detail in Section 4.

3.5. Iceberg Study Site

During January 2-3, 2011 the NBP traveled near a tabular iceberg drifting within the Dotson trough (-73.6° S, -113.5 ° W) and collected ADCP and CTD data (Figure 17; Table 3). Southerly winds prevailed and based on MODIS satellite imagery, accelerated the iceberg's drift to the northwest at ~0.3 knots. CTD stations that were in the wake of where the iceberg passed, or in areas where

currents flowed through the wake of the iceberg, experienced 'disturbed' water columns, showing an eroded WW layer due to vertical mixing of a melt-laden layer and mCDW.

3.5.1. Extent of Iceberg Mixing and Water Mass Modification

The intensity of water column mixing by a drifting iceberg is highly dependant on local winds and currents. Our data suggest that within 10 km downstream of the drifting iceberg, waters were 'disturbed' (vertically mixed) compared to surrounding polynya waters; that is, the deep-keeled iceberg caused mixing-up of the melt-laden layer and mCDW, thus eroding the overlying WW layer and pycnocline (Figure 18). As the iceberg drifted to the NW, it mechanically mixed the water column, creating a wake of heterogeneously mixed water masses in its path.

The iceberg-enhanced vertical mixing can best be seen in the temperature and salinity profiles of CTD81 and TMC31 (Figure 18). Local currents reaching CTD81 had passed through the wake of the iceberg, thus delivering the vertically mixed waters observed at this location.. Sharp temperature gradients indicate mixing of mCDW and WW by the keel of the iceberg, thus effectively warming and salinifying WW (Figure 18). TMC31 was 0.5 km to the SE of the iceberg and directly in the iceberg's wake. TMC31 was similar in shape to CTD81 but had a less-eroded WW layer. The differences between the temperature profiles at CTD81 and TMC31 are likely because we sampled TMC31 shortly after the

iceberg passed. In short, both CTD 81 and TMC31 exhibited eroded pycnolcines and WW layers, vertically mixed with melt-laden water and mCDW between 200-600 m.

Outside the mixing influence of the drifting iceberg were CTD83 and CTD84. CTD83 was 1 km NW of the iceberg (i.e., upstream of the iceberg drift trajectory) and CTD84 was 15 km to the east of the iceberg. Both were in quiescent, typical ASP waters. The data profiles from CTD83 and CTD84 had a 'check mark' shape when displayed in T-S space (Figure 18), indicating a well-defined Tmin and WW properties. Unlike CTD83 and CTD84, data from CTD81 and TMC31 displayed in T-S space intermittently extended toward the Gade line (i.e., the prescribed mixing line between fresh water and mCDW). Although data from CTD81 and TMC31 did not overall lie as close to the Gade line as data from the DIS outflow (TMC29), meltwater fractions were similar (see 3.5.2).

3.5.2. Calculated Meltwater Fractions near the Iceberg

Measurements from CTD's in the wake of where the iceberg drifted show elevated MWF's that nearly equal DIS outflow values (Figure 19). All calculated MWF profiles converge at ~500 m, the same depth Wåhlin et al. (2010) measured an outflow of a presumed mixture of melt-laden water and mCDW at the shelf break of the Dotson trough. Low MWF's at depth for CTD's 81, 83, 84 and TMC31 are representative of mCDW not (yet) mixed with meltwater. CTD83 and CTD84 also have MWF's close to zero between 300-400 m, representing

unmodified WW (i.e., not yet mixed with meltwater). In the iceberg 'disturbed' water we could not distinguish nor quantify how much meltwater was of iceberg or DIS origin.

For further comparison, we also note that both CTD81 ('disturbed') and CTD84 ('undisturbed') shared a similar location on the eastern bank of the Dotson trough and should have had very similar water column properties. However, CTD81 exhibited mixed conditions and elevated MWF's at the same depths CTD84 had a distinct WW layer and correspondingly low MWF's. Still, both CTD81 and TMC31 contain data at ~300 m more typical of unmodified WW. This data appears as a deviation away from the Gade line in T-S space, and lies closer to typical WW conditions, as expressed by CTD83 and CTD84.

Iron concentrations at TMC31 (and at TMC30, which was taken in the same location and just after CTD81) were elevated compared to typical ASP conditions but were lower than the DIS outflow (Figure 20). Iron scavenging is the likely reason for the decreased dFe values at the iceberg study site as compared to the DIS outflow (R. Sherrell, Rutgers University, pers. comm.). As the iceberg drifted, it released unknown quantities of dFe and other trace metals through in situ melting, and as described above, also by vertically mixing of melt-laden, iron-rich water from depth. TMC30 and TMC31 have lowest dFe concentrations at ~300 m, the same depth at which we also identified less modified WW (as described above). Without dFe contributions associated with

the drifting iceberg (i.e. a water column consisting of WW overlaying mCDW without any mixing processes), we would expect a typical ASP iron profile to look like Station 6.

3.6. A Melt-laden Layer throughout the Dotson Trough

Based on our estimates and previous observations, melt-laden water was also detected beyond the immediate outflow area in front of the DIS (e.g., Figure 15) and appeared to extend throughout the Dotson trough. Previously, Wåhlin et al. (2010) noted a melt-laden layer between 450-600 m at the northern extent of the Dotson trough. We substantiate these findings by calculating MWF's in the Dotson trough (Figure 21), which qualitatively indicates a melt-laden layer at similar depths. (We say 'qualitatively' because of the sensitivity of the MWF calculation to selected 'ambient' T/S values for WW/CDW as discussed in Section 2.4.) Nonetheless, a distinct melt-laden layer (~5 ppt meltwater) appears to extend from the DIS at mid-water column depths (where the highest values are found at ~200-400 m) down to ~600 m and reaches the shelf break between 300-400 m, roughly following the 27.6 isopycnal. A similar melt-laden layer was noted throughout the nearby Pine Island Glacier trough system (P. Dutrieux, British Antarctic Survey, pers. comm.).

The extension of the melt-laden layer to the shelf break is further substantiated by iron measurements at the shelf break station. At that location, we observed elevated dFe concentrations at ~400 m, the same depth with

correspondingly elevated MWF's (Figure 20 and Figure 21(a)). The significance of detecting a melt-laden layer throughout the Dotson trough is the potential for vertically mixing this source of iron into the mixed layer to potentially fuel biological production. We already documented a case of strong vertical mixing by icebergs (Section 3.5), but other processes such as strong wind mixing or seasonal water column overturning could also bring the iron-rich meltwaters up into the mixed layer.

Wåhlin et al. (2010) investigated on/off continental shelf exchange of mCDW, whereby warm mCDW presumably flows onto the shelf along the eastern bank of the Dotson trough, interacts with the DIS, and then flows off the shelf along the western bank. New hydrographic data from NBP1005 substantiate and expand on Wåhlin et al (2010) findings by identifying mCDW near the sea floor throughout the Dotson trough. Using LADCP, Wåhlin et al. (2010) noted a <10 cm/s southward current near the sea floor in the northern part of the Dotson trough, transporting between 0.3-0.4 Sv of mCDW toward the continent. We confirmed that ~0.6°C mCDW arrives at the DIS at depth and that there is a strong outflow of melt-laden water (enhanced at mid-water column depths but also detected down to 600 m) that appears to extend offshore in a layer roughly corresponding to the 27.6 isopycnal.

We infer that the returning northward flow of melt-laden water through the Dotson trough is likely diffuse, broad and slowly flowing. The NBP1005 data

captured at the DIS outflow also provided ocean current measurements of the melt-laden layer, and those data indicated a >0.20 m/s northward outflow. Back of the envelope calculations show that the DIS outflow, centered at -113.33° W, discharges ~0.16 Sv (0.2 m/s * 2000 m * 400 m) of melt-laden outflow. Although this does not account for all the inflow of mCDW that Wåhlin et al. (2010) describe, it does indicate that a large portion of the melt-laden, mCDW mixture exited at this location. Lower quantities of melt-laden outflow also existed between 400-600 m (Figure 15) across the DIS (i.e., east of the strong outflow area), which could potentially close the inflow/outflow budget. Although these bulk outflow calculations are based on few data points and represent a grossly simplified outflow scenario, the magnitudes of outflow and inflow seem plausible. (We also acknowledge that this calculation did not for example take into consideration multi-year data, tidal forcing, wind forcing or internal wave dynamics.)

4. Discussion

4.1. Comparing hydrographic transects in front of PIG and DIS

Located 325 km to the east of the DIS, PIG is a popularly studied, actively retreating glacier in the Pine Island Bay area. There are many similarities between the DIS and PIG including: the entrance of mCDW onto the continental shelf at trough locations, how mCDW flows at depth through each trough system to the ice shelf grounding lines, sub-ice shelf melting processes and how a melt-

laden water mass exits from under each ice shelf in a geostrophically driven current. The most significant difference between each location is that warmer mCDW reaches the glacial grounding lines of PIG compared to DIS, driving rapid ice shelf retreat (Jacobs et al., 2011).

Jacobs et al. (2011) analyzed CTD stations repeated from several different cruises to the front of PIG to identify water mass interactions with the ice shelf. The most distinct features across this transect in front of PIG were a large pool of mCDW >600 m and a melt-laden outflow at the southern/western boundary. After noting similar features in front of the DIS (e.g., Figure 13), we directly compared water mass properties from CTD's taken in front of each ice shelf (Figure 22). The DIS was distinctly cooler at all depths compared to PIG. At PIG, mCDW was ~3°C above the in situ freezing point (Tf) and 34.7 psu whereas at DIS, mCDW was ~2.1 > Tf and 34.55 psu. Cooler and fresher mCDW at DIS indicates a higher degree of CDW modification along the Dotson trough compared to the Pine Island Bay trough system. Warmer mCDW reaching the grounding line of PIG would presumably lead to a significant melt-laden layer, discussed further in Section 4.3.

4.1.1. Comparing melt-laden outflows at PIG and DIS

Outflow data from both the DIS and PIG appeared linear in T-S space and fell close to the Gade line, indicating a mixture between meltwater and mCDW (Figure 22). Specific slope and y-intercept of the Gade line depends on the two

end members (i.e., meltwater and CDW) at each ice shelf (here differing primarily in the CDW properties), thus the melt-laden and mCDW mixture exiting at PIG was overall warmer and saltier. Only the CTD's recorded at each outflow have data that lie near the Gade line; indicating, within the spatial sampling of the CTD's, that the outflow is mostly concentrated in a narrow region along the western/southern boundaries of each ice shelf.

The DIS outflow was at all depths cooler than the PIG outflow from a combination of highly-modified CDW reaching the ice shelf via the Dotson trough, with additional possible contributions from outflow waters emanating from PIG (and other upstream ice shelves) by means of a coastal current. The DIS outflow, unlike the PIG outflow, had a 100 m surface mixed layer from recent seasonal warming, but this difference is likely due to sampling time of each cruise (~mid December versus late January, respectively). The location of the outflow at PIG is also much deeper and thus shows at full depth the warmer, saltier values of less-modified CDW (i.e., less compared to mCDW in the Dotson area). In the upper ~300 m however, the DIS outflow is distinctly fresher than PIG outflow, in the depth range corresponding to the enhanced melt-laden outflow detected at DIS (Figures 12 and 15).

Since 1994, PIG has experienced ~50% increase in meltwater production and stronger sub-ice shelf circulation (Jacobs et al., 2011). Calculated outflow transport at PIG is 0.403 Sv (Jacobs et al., 2011), whereas back-of-the-envelope

calculations at DIS infer a 0.16 Sv outflow (Section 3.6.). Currently there have not been any reported LADCP measurements at the DIS, so it is not possible at this time to determine changes in outflow velocities over time. However, since 2007 we have noted a warming at the DIS (see next section) and a similar increase in meltwater content in the water column (Section 4.3), which might indicate an increase in outflow transport as well.

4.2. Hydrographic changes at the DIS outflow since 2007

The DIS outflow has become increasingly warmer and saltier at most depths since 2007 (Figure 23). Data representing each year was collected within 0.25 km radius and occurred during late spring (2011) and summer (2007 and 2009). When displayed in T-S space, DIS outflow data from 2011 appears closest to the calculated Gade line, representing a greater mixture of meltwater and mCDW (Figure 23, inset). Since 2007, the upper 200-300 m has warmed the most by ~0.5°C, indicating a greater concentration of upwelled (freshened) mCDW in the melt-laden outflow.

DIS outflow waters at the sea floor were warmer in 2009 and 2011 compared to 2007. An increased volume of mCDW reaching the DIS in 2009 and 2011 is potentially the reason for warmer and saltier bottom temperatures. Both austral spring-summers in 2009 and 2011 coincided with La Niña conditions and a positive SAM state, whereas 2007 coincided with El Niño conditions and a negative SAM state. Stronger westerly winds at the Amundsen

Sea continental shelf break associated with La Niña/+SAM could have potentially forced more mCDW onto Amundsen Sea embayment and into Dotson trough (Thoma et al., 2008), thus leading to warmer, saltier conditions at the DIS outflow.

Despite such yearly variability associated with ENSO/SAM, time series analyses of temperature and salinity conditions in front of PIG also showed warming and salinifying conditions between 1994-2009. Jacobs et al. (2011) associated rapid melting of PIG with increased presence of mCDW reaching the grounding line and stronger sub-glacier circulation. Historical data at the DIS are fewer than at PIG, but similar warming and salinifying trends indicate increased presence of mCDW flowing under both ice shelves, which in turn fuels increased melt as indicated in the next section.

4.3. A Melt-laden presence at PIG and DIS outflows

Given that the simplified sub-ice shelf dynamics at both the DIS and PIG consist of inflowing mCDW at depth along the eastern boundary of the trough system and a buoyant, geostrophically steered outflow mixture of melt-laden water and mCDW along the western/southern boundary (Potter et al. 1988, Jenkins et al., 2008, Jacobs et al., 2011), we calculated and compared meltwater fractions of both outflows (Figure 24). Below 600 m at the PIG outflow, there are near-zero MWF's, which represent least modified (i.e., by meltwater

freshening) mCDW. This is consistent with deeper depths in the trough system at PIG than at DIS, thus accommodating the denser (saltier) mCDW.

Calculated MWF's at the DIS outflow in 2011 were greatest in the ~100 to 300 m depth range (Figure 24), reaching MWF's > 20 ppt that were notably higher than at PIG. Calculated MWF's from 2007, 2009, and 2011 also indicate a progressively more melt-laden DIS outflow. Following the discussions from above, increased MWF's could potentially be caused by warmer and/or greater amounts of mCDW interacting with the DIS. Increased melt-laden content in the DIS outflow also has biological consequences, since it would point to a concurrent increase in dFe delivered to the ASP region.

If we were to vertically integrate the MWF's at DIS (for 2011) and at PIG (for 2009) over ~100m to 600m, we would see overall similar meltwater content at both PIG and DIS. Indeed, the depth distribution of MWF's at each outflow is different because of the differences in the ambient mCDW being modified by the meltwater. Since mCDW is warmer and saltier at PIG, the meltwater outflow is relatively denser. Consequently, there are greater MWF's in the ~300-500 m depth range at PIG as opposed to the greater MWF's at DIS in the ~100-300 m depth range. However, the fact that they both show similar integrated meltwater content is interesting, because the melt potential for a given amount of mCDW must be less under DIS than under PIG given the cooler ambient conditions of the mCDW entering under DIS.

However, the DIS is a considerably larger ice shelf than PIG, so melting may occur over a larger sub-ice shelf area, facilitated by the 'lighter' ambient mCDW entering the DIS. In other words, the flow of mCDW under DIS may interact longer with the ice shelf base and not detach as quickly after generating melt at the grounding line, as has been inferred for the sub-ice shelf circulation under PIG (Jenkins et al., 2010). To better constrain these questions and comparisons, we need more such studies in front of ice shelves as described here, particularly studies using Lowered ADCP observations, to better define inflow and outflow boundaries, velocities, and meltwater export.

4.4. Comparing drifting icebergs in the ASP to the Weddell Sea

Water mass mixing by drifting icebergs in the Dotson trough region of the ASP differs from what was reported by Stephenson Jr. et al. (2010) in the western Weddell Sea. In general the stratification and water mass properties and depth distributions were very different between the two iceberg study sites, which consequently resulted in different mixing or modification of water masses affected by iceberg drift. The iceberg in the ASP was about 3 km by 1 km with an estimated keel depth between 340-450 m, whereas the iceberg in the western Weddell Sea was 35 km by 6 km with a measured keel depth of 190 m. The ambient conditions at the iceberg keel depth in the ASP were -1.8°C and 34.15 psu, indicative of cold, fresh WW. However, ambient conditions at the iceberg keel depth in the western Weddell Sea were -0.25°C and 34.6 psu, indicative of

warm, salty CDW. Overall warmer WW and shallower access to mCDW in the western Weddell Sea could cause a higher concentration of in situ iceberg melting.

At the ASP study site, WW extended deeper and was colder and fresher than at the western Weddell study site (Table 4). Although the mCDW in the ASP was warmer and saltier than in the western Weddell, it resided deeper in the water column. However, as established above, at the ASP study site, there was a melt-laden layer at the base of the pycnocline, which was within reach of the iceberg keel. Thus, in the ASP region mixing by the iceberg extended into this melt-laden layer, which relative to waters at 300-400 m in the western Weddell, were cooler and fresher (but still warmer and saltier than ASP WW). We therefore infer that there was considerably less in situ iceberg melt in the ASP region due to the cooler ambient conditions at 300-400 m. Nonetheless we observed injection of Fe-laden melt waters into the WW layer at the ASP study site, mainly contributed by the melt-laden layer at the base of the pycnocline, with some amount due to in situ melt, but again the latter being considerably less than what was observed in the western Weddell.

Stephenson Jr. et al., (2010) noted that CTDs profiles close to the drifting iceberg (<5 km) in the Weddell Sea exhibited a completely eroded WW layer from upwelled, warmer waters. The iceberg study site in the ASP was similar in that with increasing distance from the iceberg, water mass modification (i.e.

partially eroded WW layer) decreased. Drifting icebergs in the ASP have not been directly studied for their influence on biological productivity, but it is inferred that they would act as 'hot spots' and 'stirrers', inducing some in situ melt while also mixing up the melt-laden layer. The end result would be the same, a delivery of dFe and other micronutrients into the surface mixed layer to help fuel and enhance biological productivity (Neshyba, 1977; Smith et al., 2007).

4.5. Implications

4.5.1. Other Potential Sources Fueling High productivity over the Amundsen Sea Plateau

The Amundsen Sea plateau is located in the eastern ASP and consists of a shallow, broad bathymetric rise. The Amundsen Sea plateau has a similar depth (<400 m) as the shallow banks on the Ross Sea continental shelf. Both shallow regions experience high sea ice production and deep WW layers (caused by brine rejection). Observations indicate that WW can extend to the seafloor in some areas/years when sea ice production is particularly high. Such strong winter mixing provides a mechanism for mobilizing sediments (through re-suspension) and entraining pFe and dFe into upper waters. Similar to how Sedwick et al. (2011) noted elevated pFe (benthic source) and dFe (mCDW source) at the seafloor over the central Ross Sea shelf, we too noted elevated dFe concentrations closest to the seafloor. Entrained iron either from winter mixing

of mCDW or from sediment resuspension primes the water column for a spring bloom as soon as sea ice retreats (Sedwick et al., 2011). The spring bloom quickly depletes surface dFe and makes the surface ocean iron limited. However, through intermittent vertical and horizontal exchange of 'new' dFe and 'recycling' of biogenic pFe in the surface layer, summer conditions can still be quite productive (Sedwick et al., 2011).

Multi-year sea ice and the Thwaites Ice Tongue occupy the eastern edge of the ASP over the Amundsen Sea plateau. Iron sources, in the form of microorganisms and pFe, accumulate in sea ice, which can contain iron concentrations up to 1.1-30.2 nmol/L (Lannuzel et al., 2010). When sea ice seasonally melts, it releases a steady stream of 'newly available' iron into the surface waters (Planquette et al., 2011; Sedwick et al., 2011). We noticed enhanced productivity near melting sea ice over the Amundsen Sea plateau and determined there was iron limitation in surface waters (A. Alderkamp, Stanford University, pers. comm.). Surface iron limitation does not necessarily mean that iron is not entering the area; rather phytoplanktonassimilate the 'newly available' iron very quickly and do not allow a surplus to accumulate.

Grounded icebergs were common over the Amundsen Sea plateau and were locked within the Thwaites Ice Tongue and surrounding sea ice. A theorized coastal current originating at PIG passes the grounded icebergs and underside of the Thwaites Ice Tongue, which potentially contribute to a year

round source of iron-rich water (Figure 25). It is possible that meltwater and turbulent processes near the base of the grounded icebergs could be a source of micronutrients that would eventually reach the ASP, thus causing it to be the most productive polynya (per m^2) in Antarctica (Arrigo et al., 2003).

4.5.2. Role of Eddies and Gyre Circulation in the ASP

Mesoscale eddy circulation over the Amundsen Sea plateau could lift isopycnals (e.g., Jacobs et al. 2011; Sedwick et al. 2011), making melt-laden waters and/or mCDW more accessible to wind mixing. Along the wAP, eddies are the primary mechanism transporting CDW onto the shelf break (Martinson et al., submitted). Jacobs et al. (2011) noted a cyclonic gyre circulation (~60 km diameter) in Pine Island Bay, which upwelled nutrient rich water to fuel intense phytoplankton blooms (A. Alderkamp, Stanford University, pers. comm.). Although not currently documented, a similar gyre circulation is possible in front of the DIS. Either transient eddies or gyres could upwell (miro) nutrient-rich waters into the surface mixed layer, providing favorable phytoplankton bloom conditions.

5. Conclusion

The ASPIRE cruise hydrographically surveyed the ASP and identified previously unreported water mass distribution and mixing. We documented mCDW entering onto the continental shelf in the ASP and noted that it cooled ~

1°C and freshened 0.4 psu on its route towards the DIS. At the DIS we confirmed the inferred inflow of mCDW along the eastern bank of the Dotson trough and an outflow mixture of melt-laden water and mCDW along the western boundary. The fate of the outflow was detected as a distinct melt-laden, iron-rich water mass between 400-600 m, extending from the DIS outflow to the continental shelf break. Elevated iron concentrations at depth within the ASP could fuel surface primary production after sporadic mixing events (e.g., by drifting icebergs, strong wind events).

Drifting icebergs in the ASP could be an overlooked mechanism for redistributing iron-rich, melt-laden waters and mCDW into the surface mixed layer. As indicated by our study, as icebergs drift through the Dotson trough region, they cause mixing of warmer, iron-rich, melt-laden waters and mCDW to shallower depths. Calculated MWF's near the iceberg study site indicated an upwelled, melt-laden layer, similar in glacial meltwater content to the DIS outflow. Although we were not able to differentiate between glacial meltwater from iceberg and DIS outflow origin, we did notice elevated dFe concentrations close to the iceberg compared to the surrounding 'undisturbed' polynya waters. Icebergs frequently pass through the ASP region, the source of which is primarily the Thwaites Ice Tongue, and could play a much larger role in entraining dFe into the mixed layer than previously reported.

The data from ASPIRE confirms that the DIS outflow experiences cooler, more-modified CDW than the PIG outflow. The warmer water under PIG would presumably create higher concentrations of meltwater compared to DIS. However, calculated MWF's at DIS and PIG outflows were similar, indicating similar relative quantities of integrated meltwater content at each location. Although we do not fully understand the sub-ice shelf dynamics at PIG and DIS, we infer that a larger area must be exposed to mCDW induced melt under DIS than under PIG given that mCDW in the Dotson trough region is distinctly cooler and fresher than in the PIG trough region.

Historical data shows that the DIS outflow has warmed since 2007. Likewise, calculated MWF's have also increased with time at the DIS outflow, indicating that either warmer mCDW could be entering under the DIS to melt more ice or sub-ice shelf dynamics have changed. Recent attention has been focused on PIG due to its rapid retreat and thinning. If warmer mCDW continues to flood into the Dotson trough, it is possible that thinning of DIS is also occurring.

Future work will focus on identifying iron delivery mechanisms to the surface mixed layer, particularly in the Amundsen Sea plateau region. The Amundsen Sea plateau had some of the highest primary production values within the ASP region and we hypothesize that it may be fueled by a melt-laden, iron-rich coastal current originating from PIG and other points east.

Figures

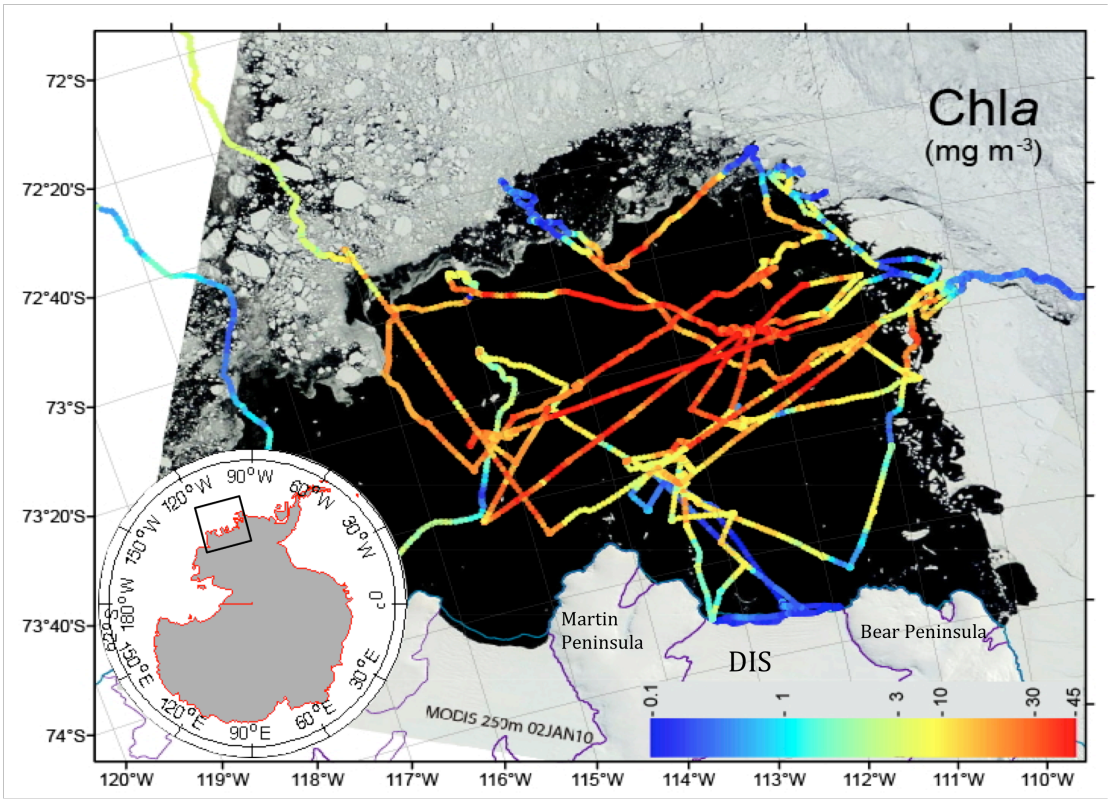

Figure 1a: MODIS satellite image of the spatial extent of the Amundsen Sea Polynya (black, open water) and surrounding sea ice (to west, north, east) and continent (to south) on Jan 2, 2011. Overlaid are underway chlorophyll-a data showing high productivity over the Amundsen Sea plateau region. Landmarks, including the Dotson Ice Shelf (DIS), are labeled (Figure created by Povl Abrahamsen.). Inset: Amundsen Sea region in Antarctica.

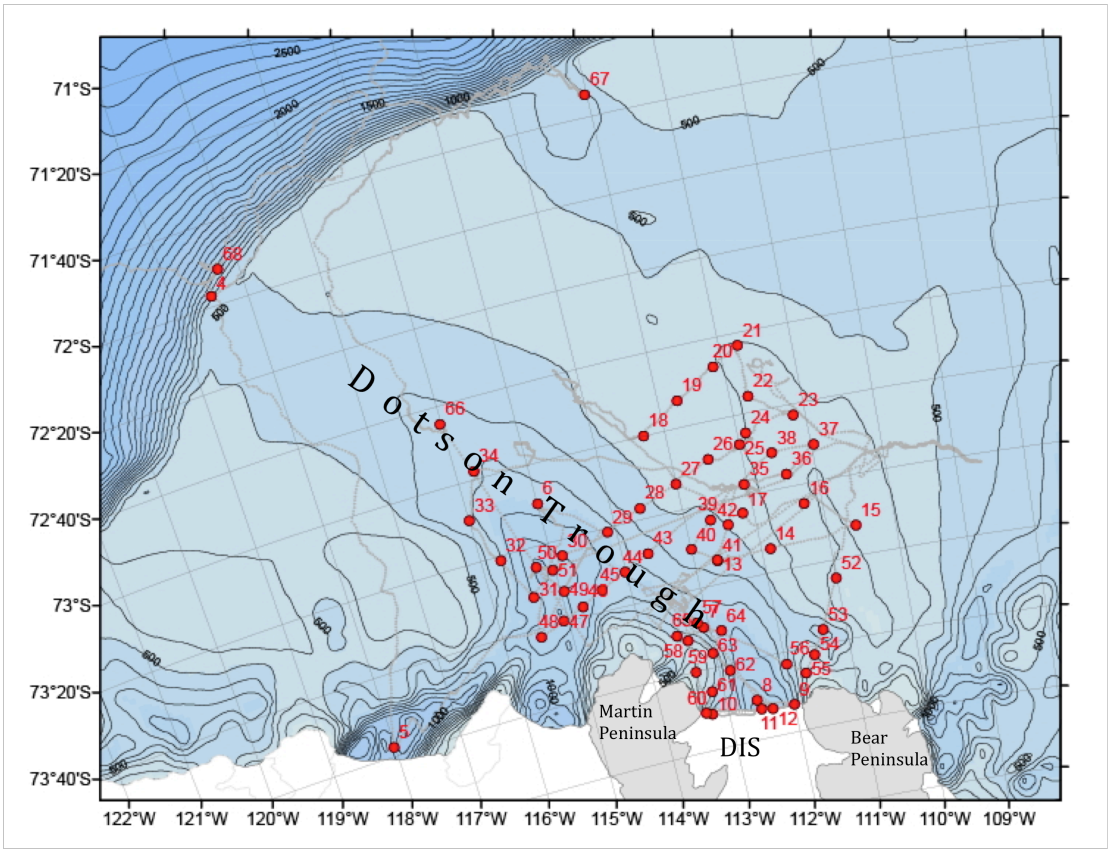

Figure 1b: Map of the Amundsen Sea Polynya (ASP) region with select bathymetric contours (black) overlaid with the cruise track (gray) and data collection stations (red dots). (Figure created by Povl Abrahamsen during ASPIRE cruise.)

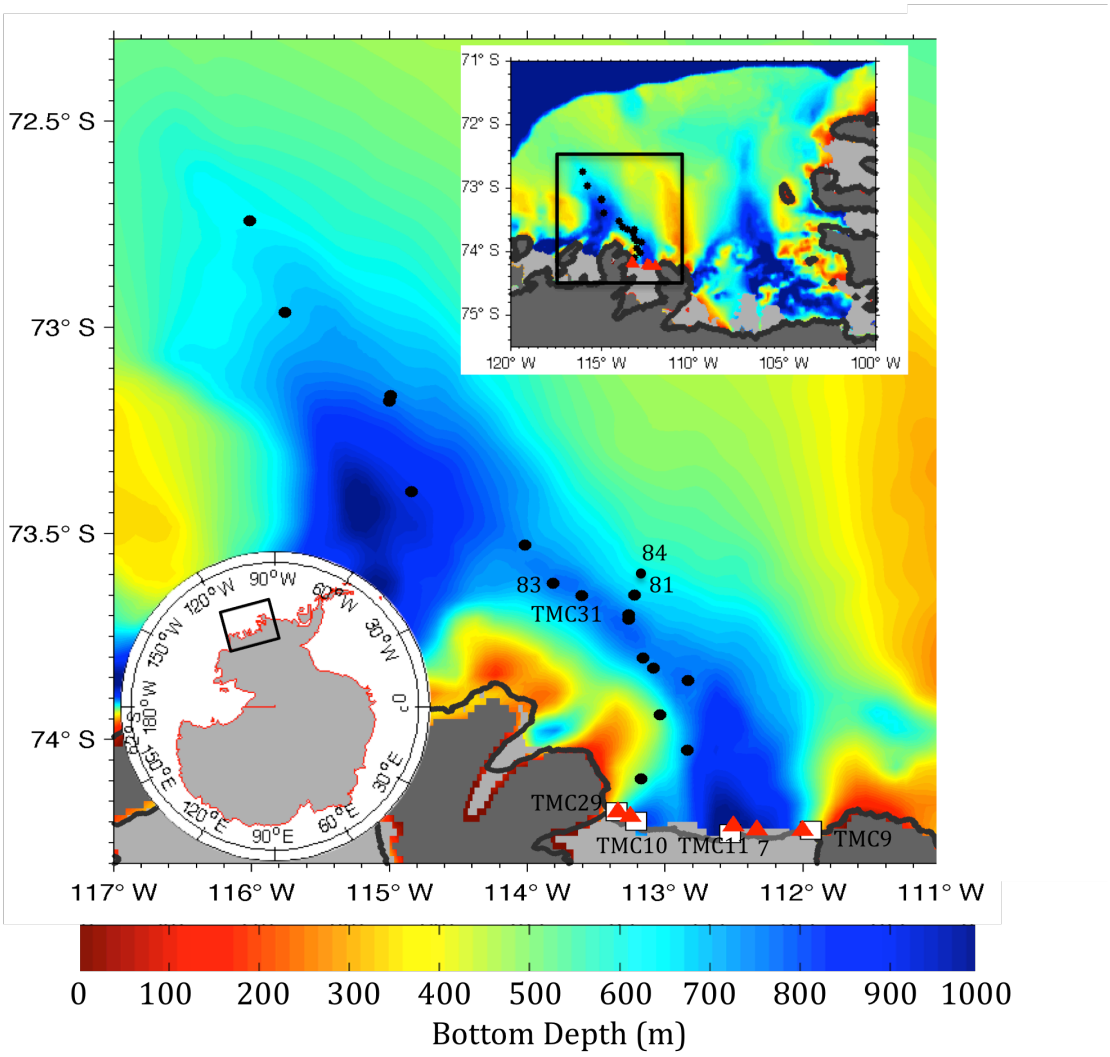

Figure 2: The Dotson trough (blue) is marked by depths >600 m. Black dots are selected CTD casts. Red triangles are DIS CTD stations. White boxes are historical data from NBP0702 and NBP0901. Inset: (top right) Regional map featuring Amundsen Sea bathymetry; (bottom left) Region in Antarctica.

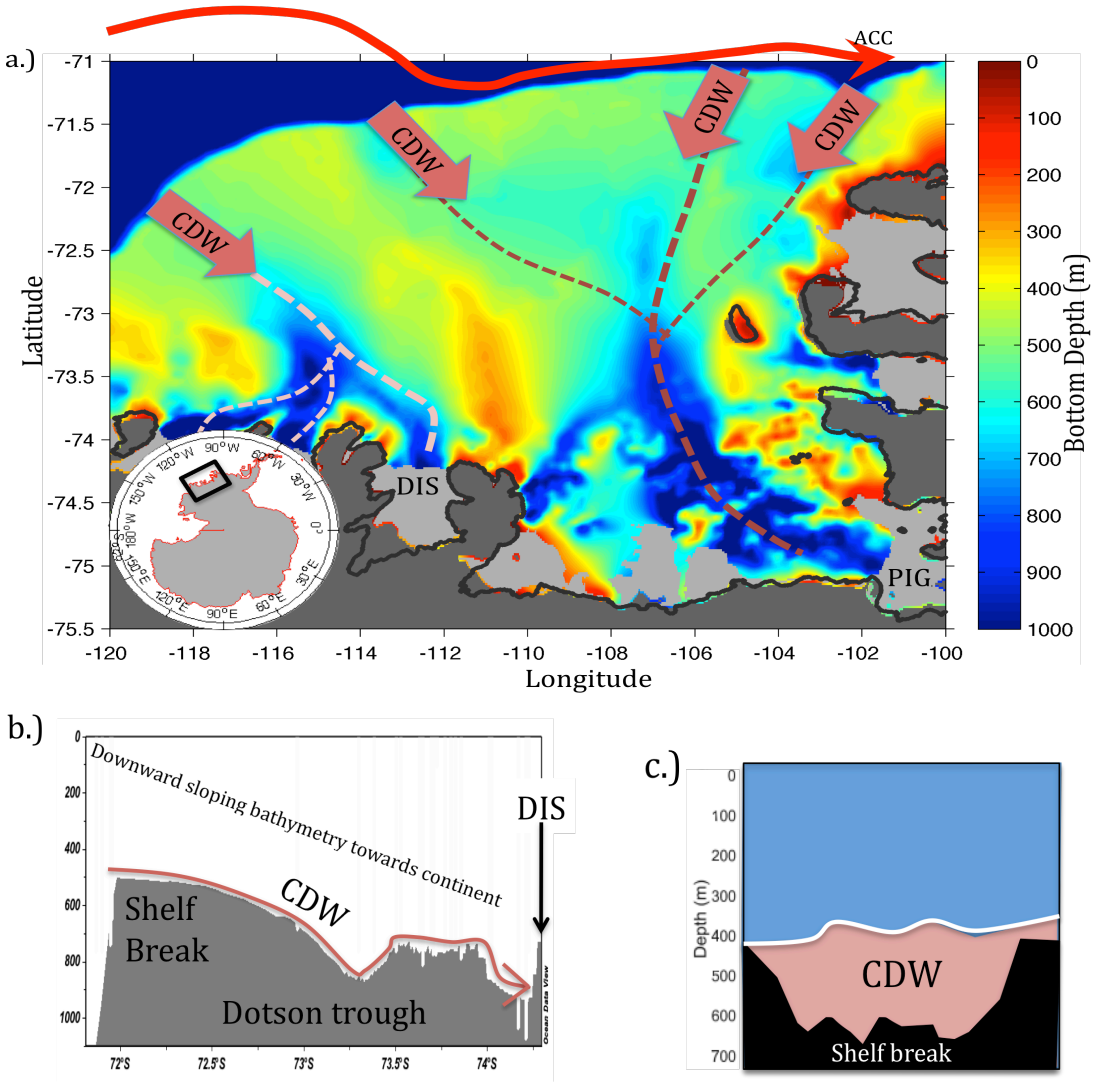

Figure 3: (a) Schematic of where CDW enters and flows onto the continental shelf in the Amundsen Sea. The Dotson trough (pink dash) experiences highly-modified CDW compared to the Pine Island Bay trough (red dash); inset (bottom left): region in Antarctica. (b) Downward sloping bathymetry allows relatively dense CDW access to the sub-ice shelf cavities and grounding lines. (c) Schematic of how at the trough regions the sill depth at the shelf break is deeper than CDW, allowing it easy access to the continental shelf. (View is looking northward at shelf break)

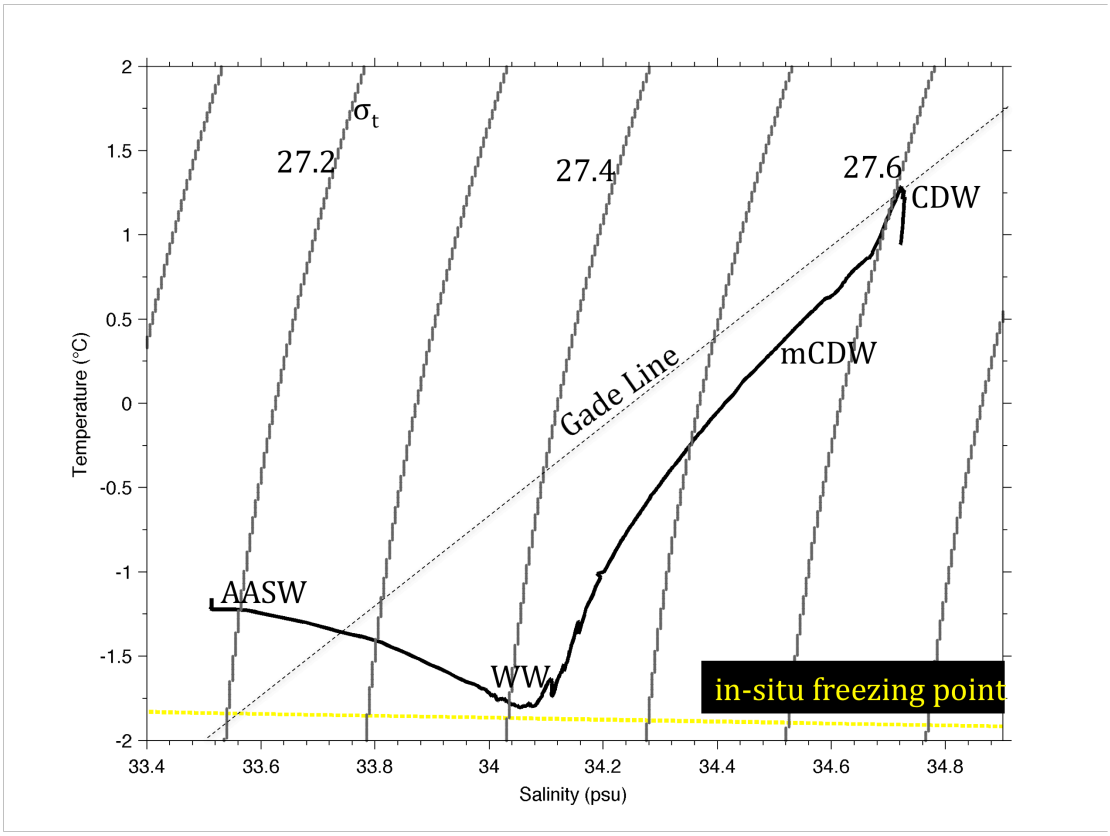

Figure 4a: Temperature (T) and salinity (S) from a CTD cast taken in the Dotson trough, showing the main water mass types displayed in TS space (solid black). Labels of water masses are as follows: Antarctic Surface Water (AASW), Winter Water (WW), modified Circumpolar Deep Water (mCDW) and CDW. Overlaid is the calculated Gade line (black dash), indicating where mixing of CDW and meltwater would occur in T-S space. The yellow dashed line is the in-situ freezing point. Isopycnals (gray) are sigma-t.

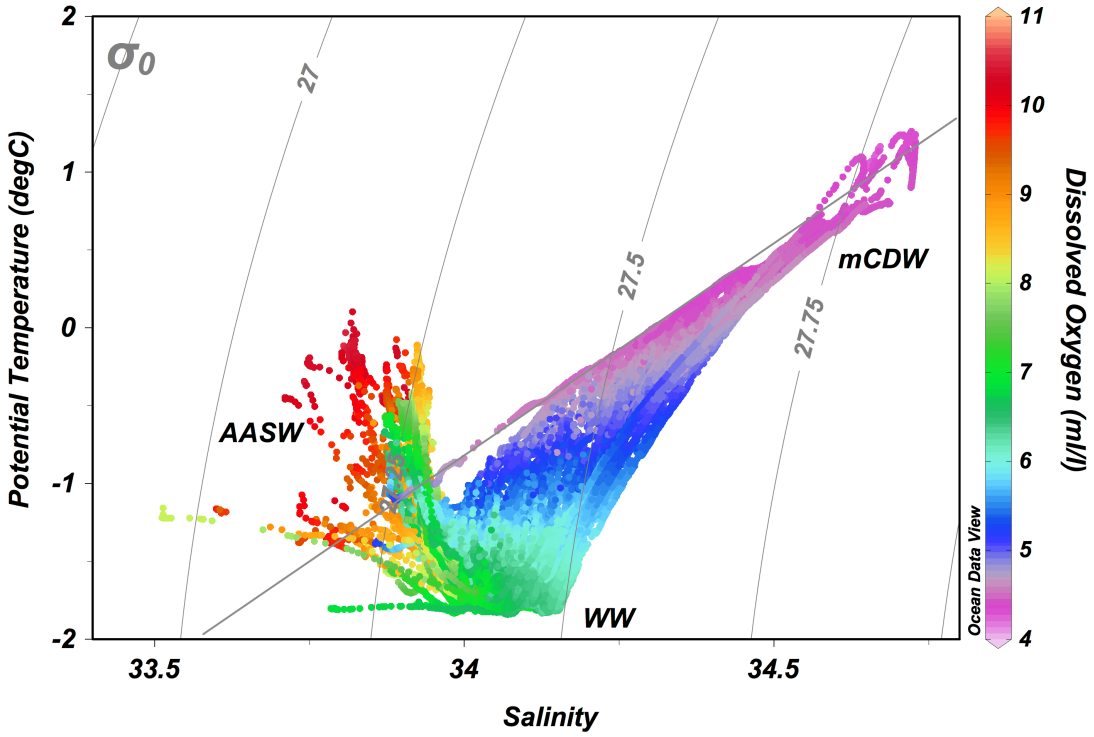

Figure 4b: T-S plot of all the CTD data collected in the ASP region, colored by dissolved oxygen concentration. Labels identify key water masses and the grey line represents the calculated Gade line.

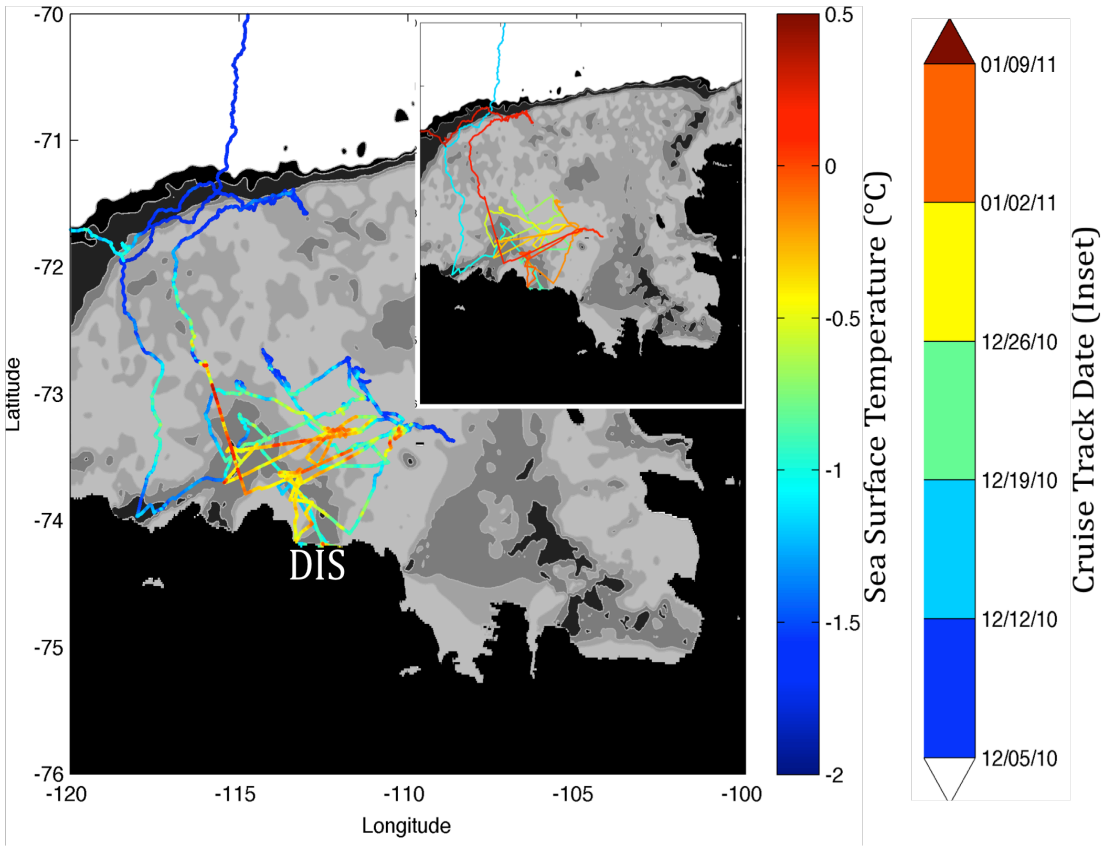

Figure 5: Shipboard underway sea surface temperature (SST) recorded throughout the ASP region. Warmer SST's were recorded in the ice-free center of the ASP, while cooler SST's were near the edges of the polynya where sea ice was actively melting, and coldest SST's were found in the heavier pack ice (to north and far east). The Antarctic continent is black and shades of darker gray represent deeper bathymetry. (Inset) Cruise track scaled to the date.

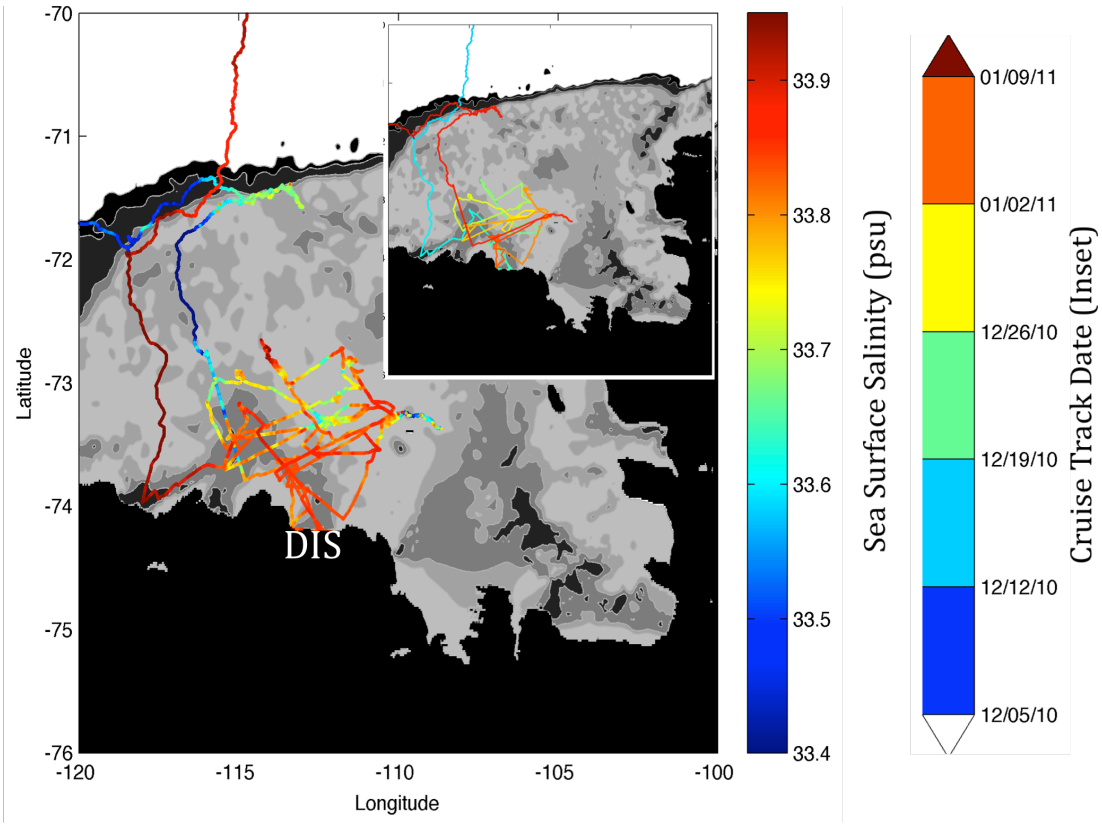

Figure 6: Shipboard underway sea surface salinity (SSS) recorded throughout the ASP. Highest SSS's were recorded upon entering the polynya where sea ice had not yet begun to melt and WW extended to the surface. Further into the ASP, surface waters were freshened from melting sea ice, creating a summer mixed layer (of AASW). Freshest surface waters were found at the polynya edges or in areas of actively melting sea ice (e.g., the outbound leg). The Antarctic continent is black and shades of darker gray represent deeper bathymetry. (Inset) Cruise track scaled to the date.

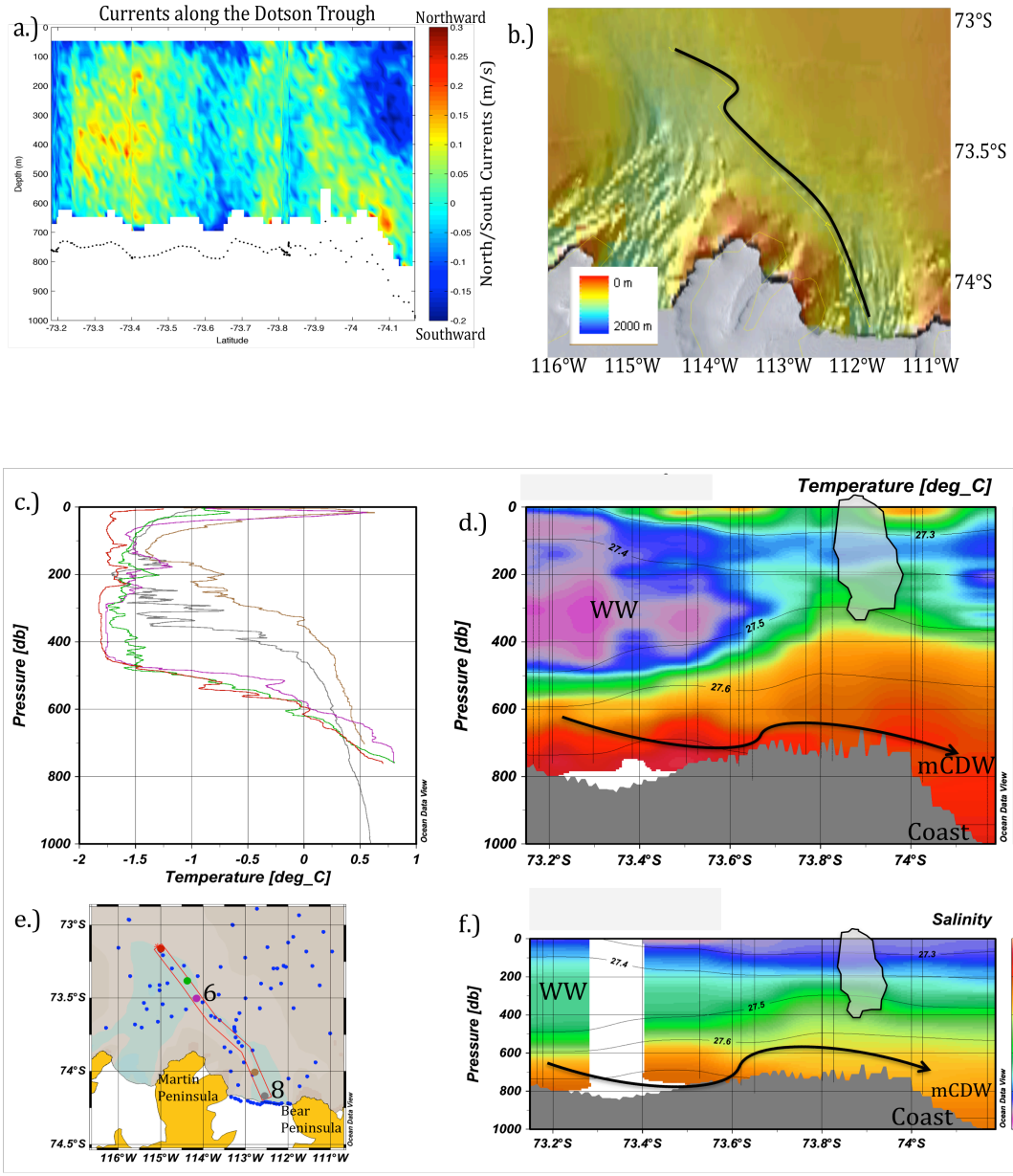

Figure 7: (a) North/south ocean currents (positive, north) observed along the Dotson trough (black dots indicate seafloor bottom); (b) bathymetry map indicating location of transect shown in (a); (c) selected temperature profiles along Dotson trough (see (e) for location); (d) temperature transect with labeled water masses and location of drifting iceberg; (e) map of CTD transect along Dotson trough (red boxed area) showing CTD casts plotted in (d) and (f) (large colored dots are casts plotted in (c); blue dots outside of boxed area are not plotted); and (f) salinity transect with labeled water masses and location of drifting iceberg. There is a data gap at 73.3°S in the salinity transect because only XBT data was collected at that location. In (d) and (f) isopycnals (black lines) are sigma-t.

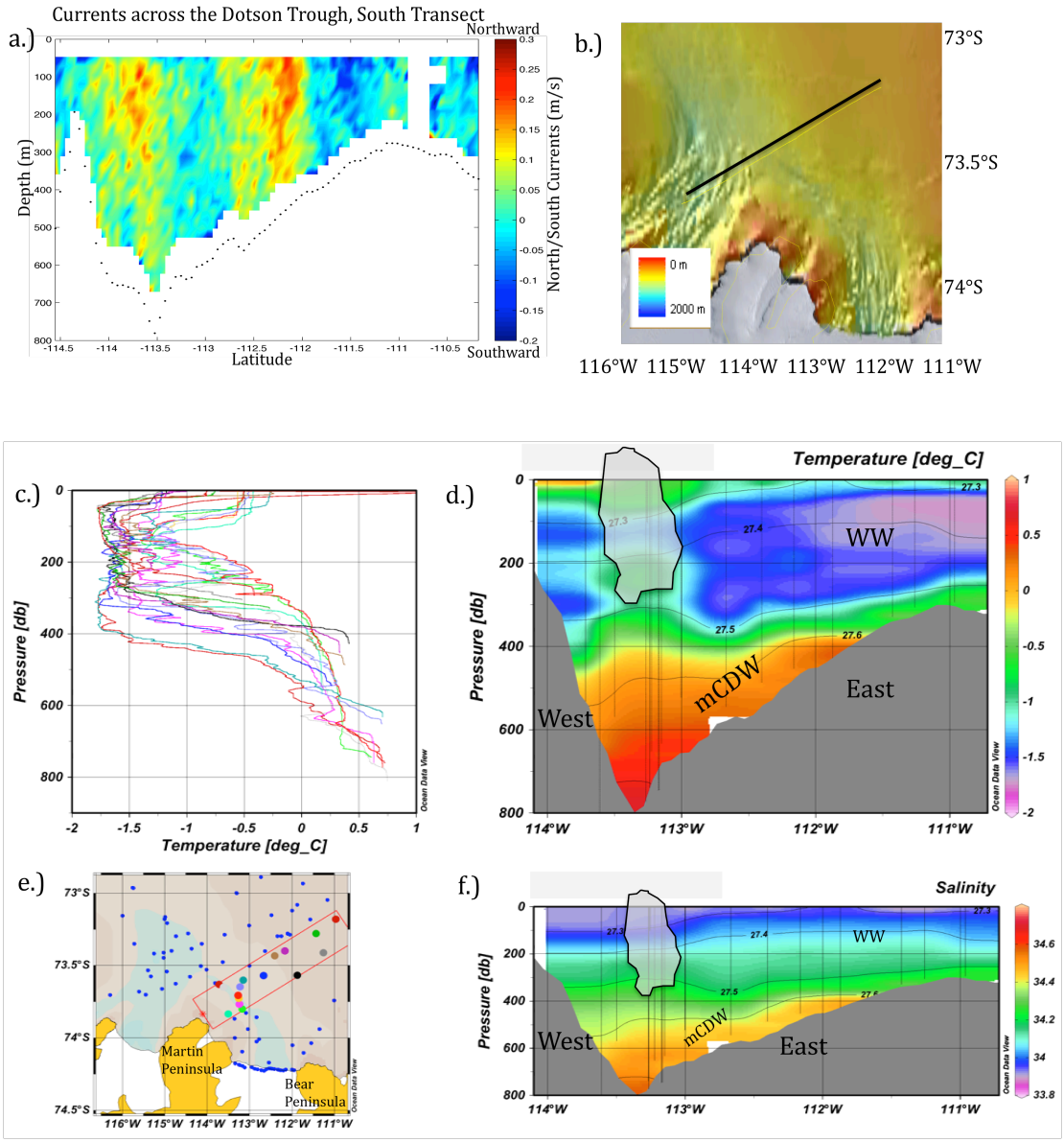

Figure 8: (a) North/south ocean currents (positive, north) observed across the Dotson trough (black dots indicate seafloor bottom); (b) bathymetry map indicating location of transect shown in (a); (c) selected temperature profiles across Dotson trough (see (e) for location); (d) temperature transect with labeled water masses and location of drifting iceberg; (e) map of CTD transect across Dotson trough (red boxed area) showing CTD casts plotted in (d) and (f) (large colored dots are casts plotted in (c); blue dots outside of boxed area are not plotted); and (f) salinity transect with labeled water masses and location of drifting iceberg. In (d) and (f) isopycnals (black lines) are sigma-t.

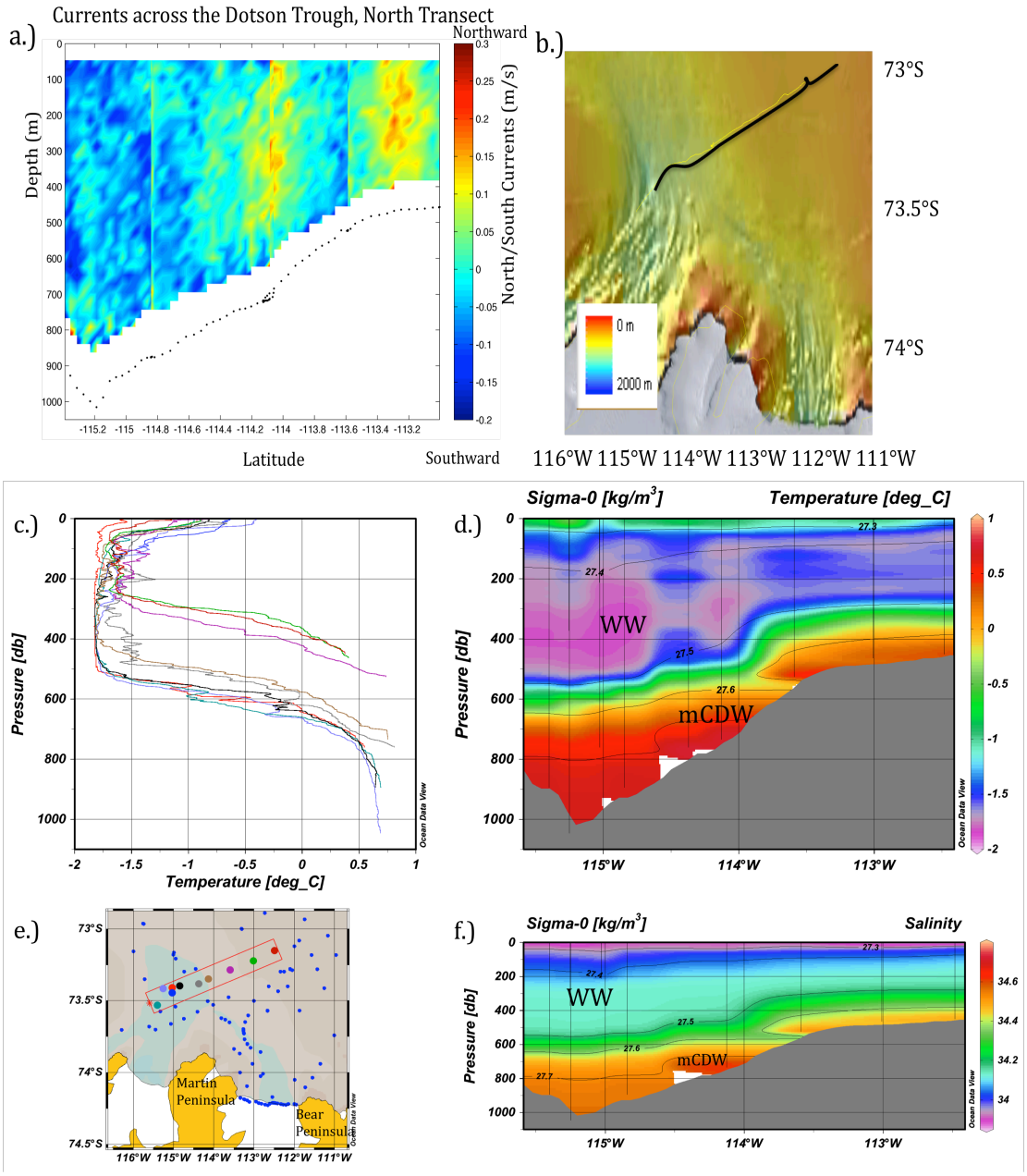

Figure 9: (a) North/south ocean currents (positive, north) observed across the Dotson trough (black dots indicate seafloor bottom); (b) bathymetry map indicating location of transect shown in (a); (c) selected temperature profiles across Dotson trough (see (e) for location); (d) temperature transect with labeled water masses and location of drifting iceberg; (e) map of CTD transect across Dotson trough (red boxed area) showing CTD casts plotted in (d) and (f) (large colored dots are casts plotted in (c); blue dots outside of boxed area are not plotted); and (f) salinity transect with labeled water masses and location of drifting iceberg. In (d) and (f) isopycnals (black lines) are sigma-t.

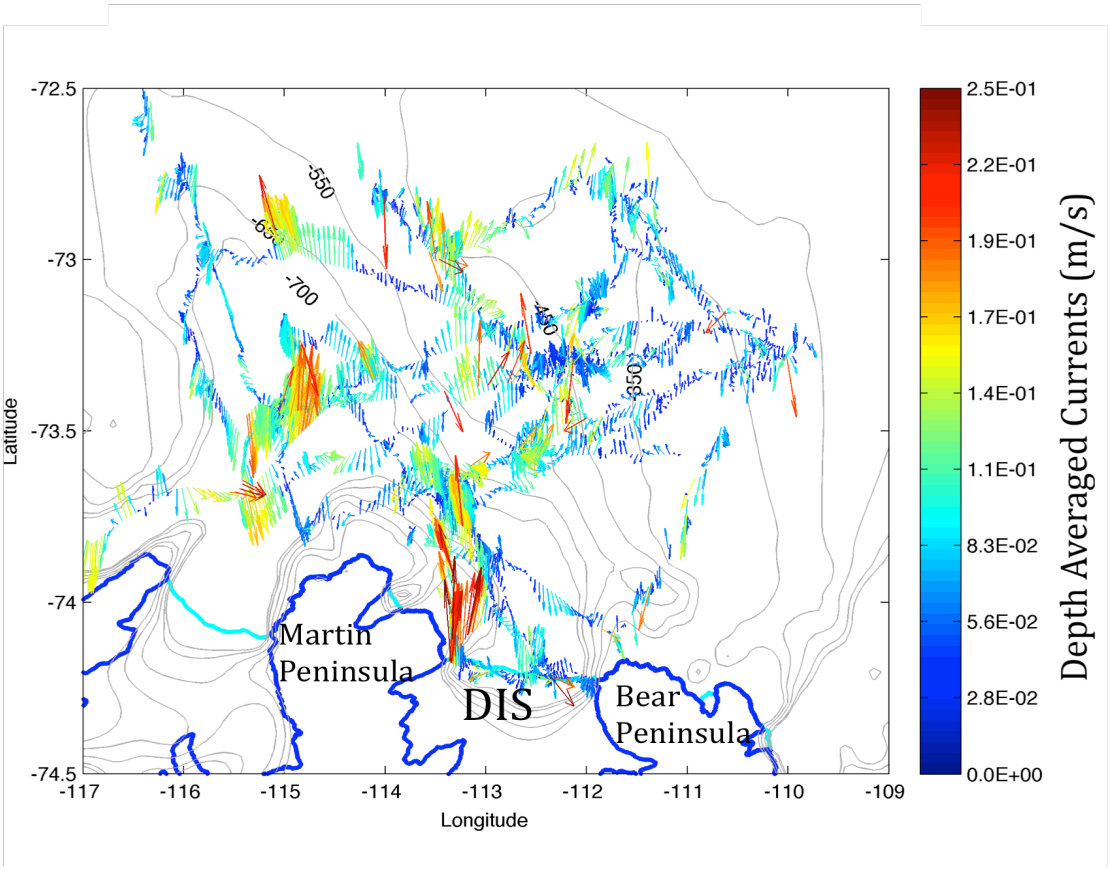

Figure 10: Underway depth averaged currents in the ASP region; shown with bathymetry contours (gray), ice shelves (cyan) and continent (blue). The data have not been de-tided, so much of the lower magnitude variability may be due to tides. However, the DIS outflow is distinct and strongly focused on the western side of the ice shelf, as expected given the inferred sub-shelf circulation (e.g., Potter et al., 1988; Jacobs et al., 2011).

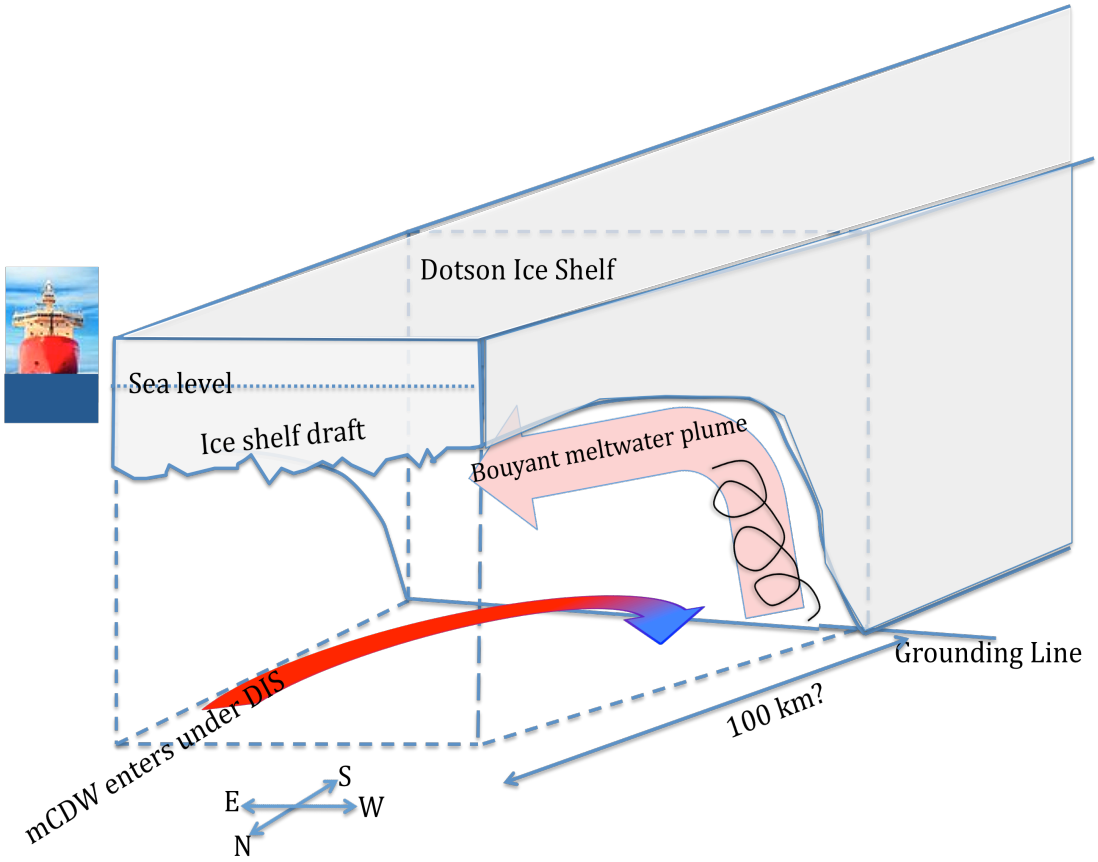

Figure 11: Schematic of how mCDW enters under the DIS and exits as a buoyant meltwater plume at the western boundary of the ice shelf. In the following Figures 12-16, all ship data (underway and XBT/CTD casts) were taken ~0.5 km seaward of the ice shelf front.

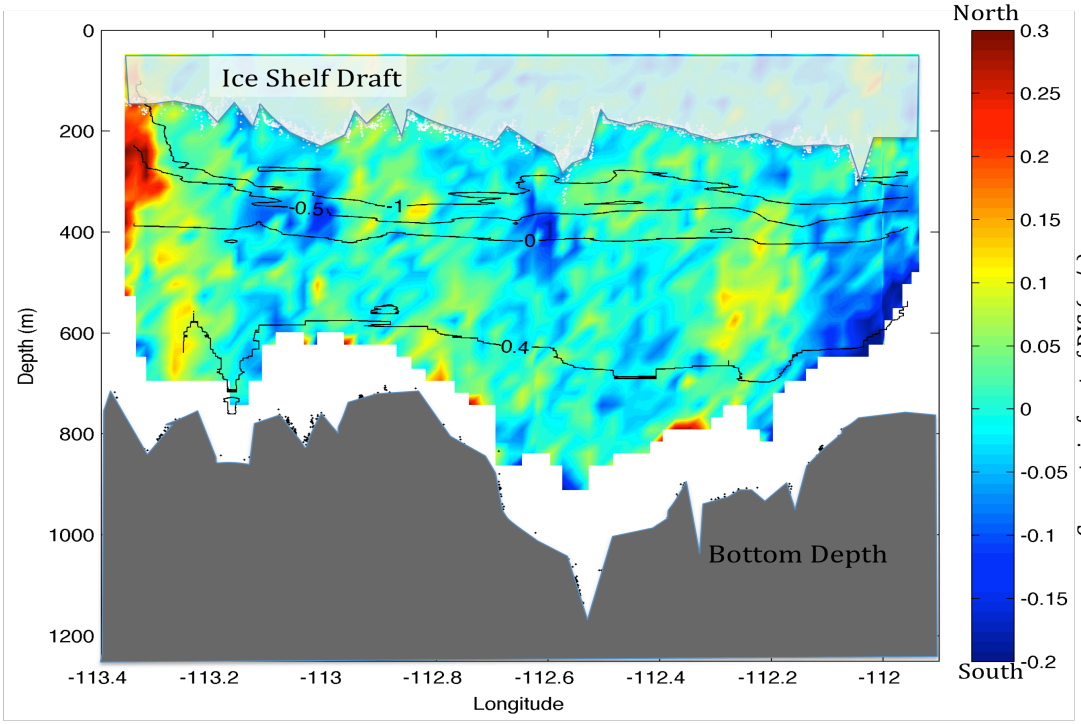

Figure 12: North/south ocean currents in front of the DIS. Ice shelf draft (top shading) thins to the west, while the bathymetry (gray shading) shows depths > 1000 m in the location of the Dotson trough (near center). Isotherms (°C, black) shoal to the west. The top 50 m and bottom 100 m (above the seafloor) contain noisy data and are excluded, although the inflow of mCDW is inferred at depth (see Figures 13 and 15), presumably enhanced on the eastern side. The ADCP current data from this transect is from December 17, 2010 09:12-14:12 and has not been detided. Banding of weak N/S currents between the enhanced eastern inflow and western outflow could represent channelized flow related to sub-ice shelf channels (Mankoff et al., 2012).

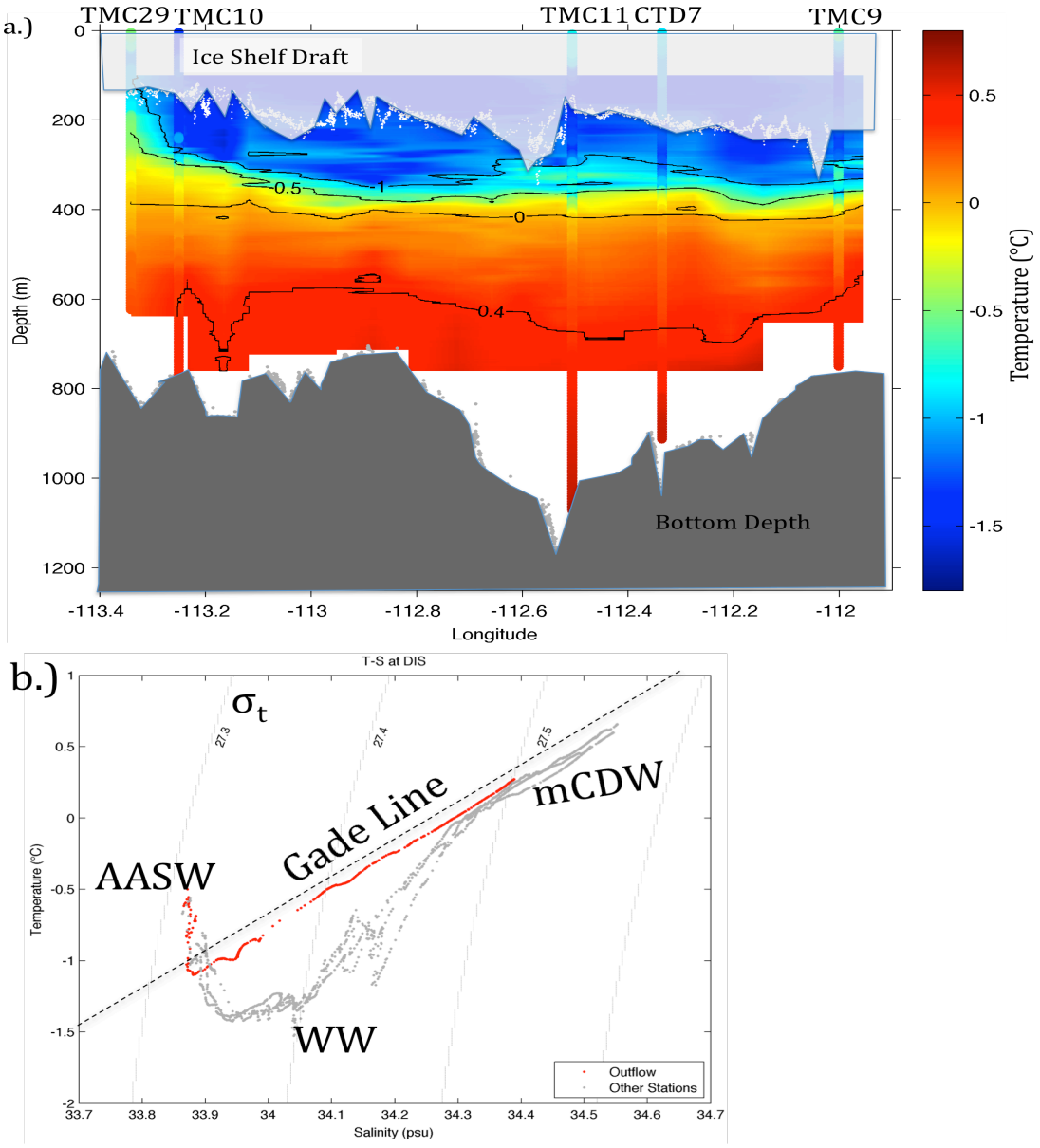

Figure 13: (a) Temperature in front of the DIS based on underway XBT data (interpolated color shading) and from 5 individual CTD casts (cast numbers given at top). Warm mCDW is present at depth, while both isotherms and ice shelf draft shoal to the west at the strong outflow region indicated in Figure 12. (b) Temperature and salinity data from the 5 CTD casts; only the DIS outflow cast (TM29, red) shows meltwater mixing with mCDW, as indicated by data falling near the Gade line (black dash). Isopycnals (gray) are sigma-t. We note that all CTD casts sampled to near bottom, including TM29, but the bathymetry shown in (a) is for the underway XBT transect, which ended to the west in deeper water than was sampled for TM29 (which was sampled to 625 m in 645 m of water).

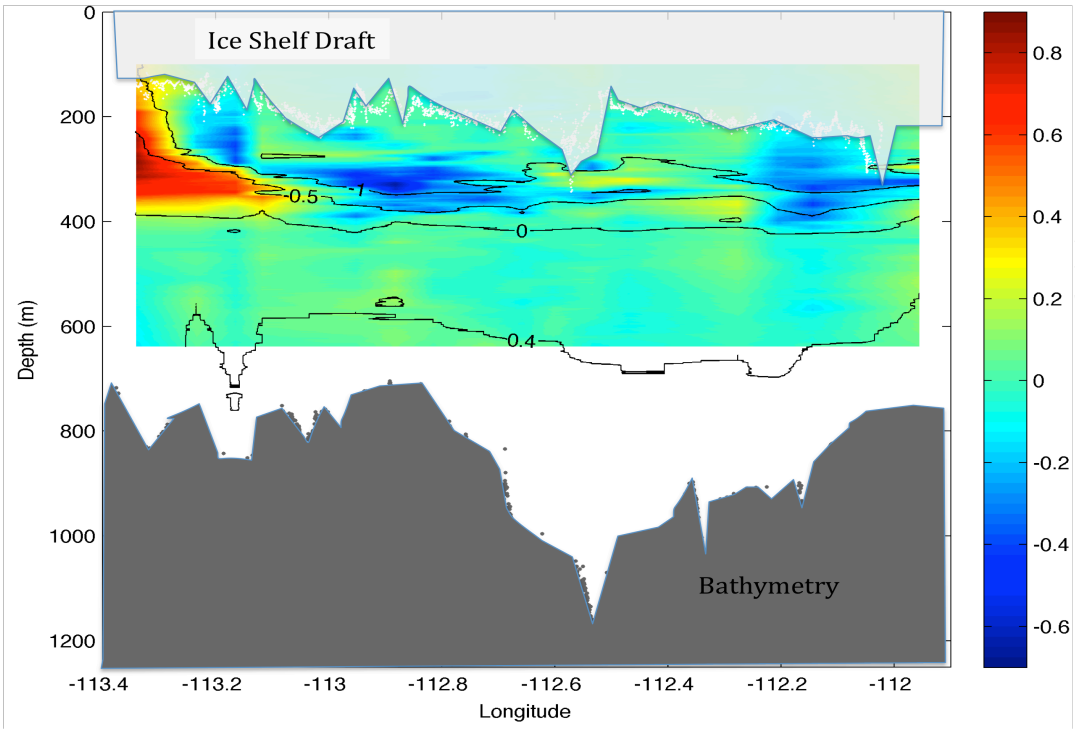

Figure 14: Derived temperature anomaly from the XBT data, determined from subtracting the depth-averaged temperature from each XBT profile. Positive temperature anomalies are situated at the outflow, where relatively warm water for that depth interval exits the DIS (see Figure 12. Anomaly data were only calculated between 100-650m. Isotherms (°C) are shown in black.

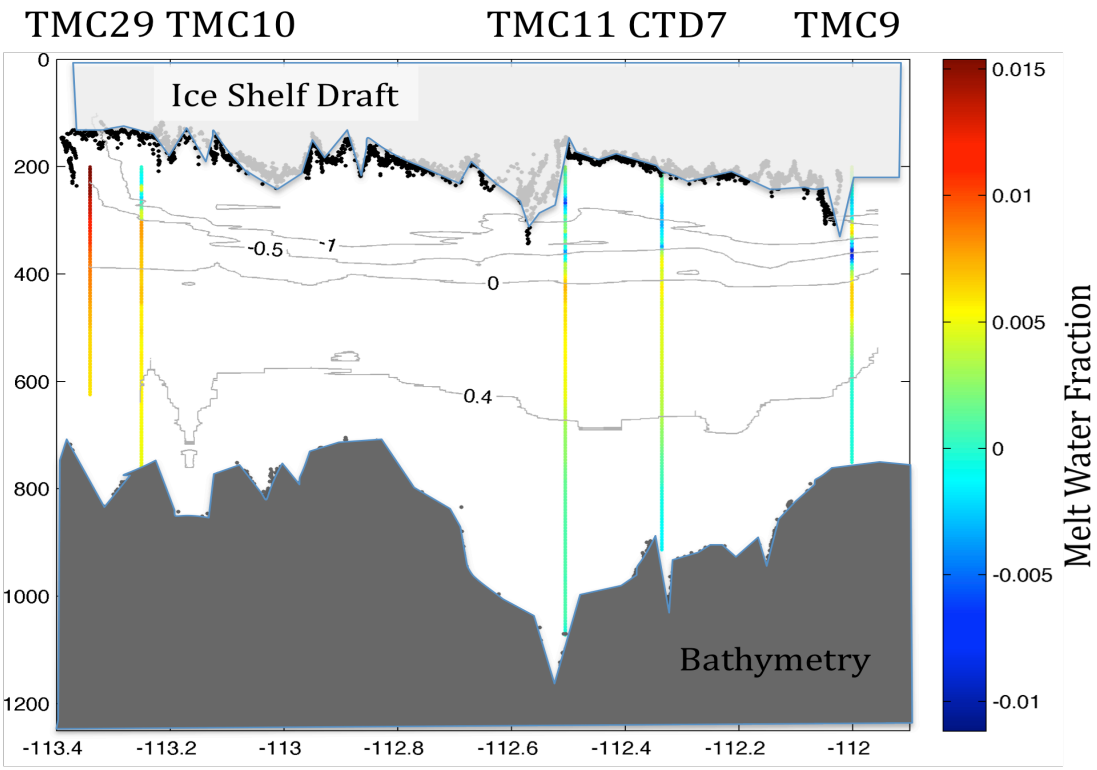

Figure 15: Calculated meltwater fractions (MWF's) at CTD stations in front of the DIS. Low MWF's at depth in the central and eastern DIS region indicate mCDW not yet mixed with meltwater. Low MWF's between 200-300 m (center, east) possibly represent undisturbed WW (i.e., not modified by meltwater). Elevated MWF's between 400-600 m could represent a layer of meltwater originating from the ice shelf grounding line. The highest MWF's are found at the outflow. Isotherms (°C) are shown in black.

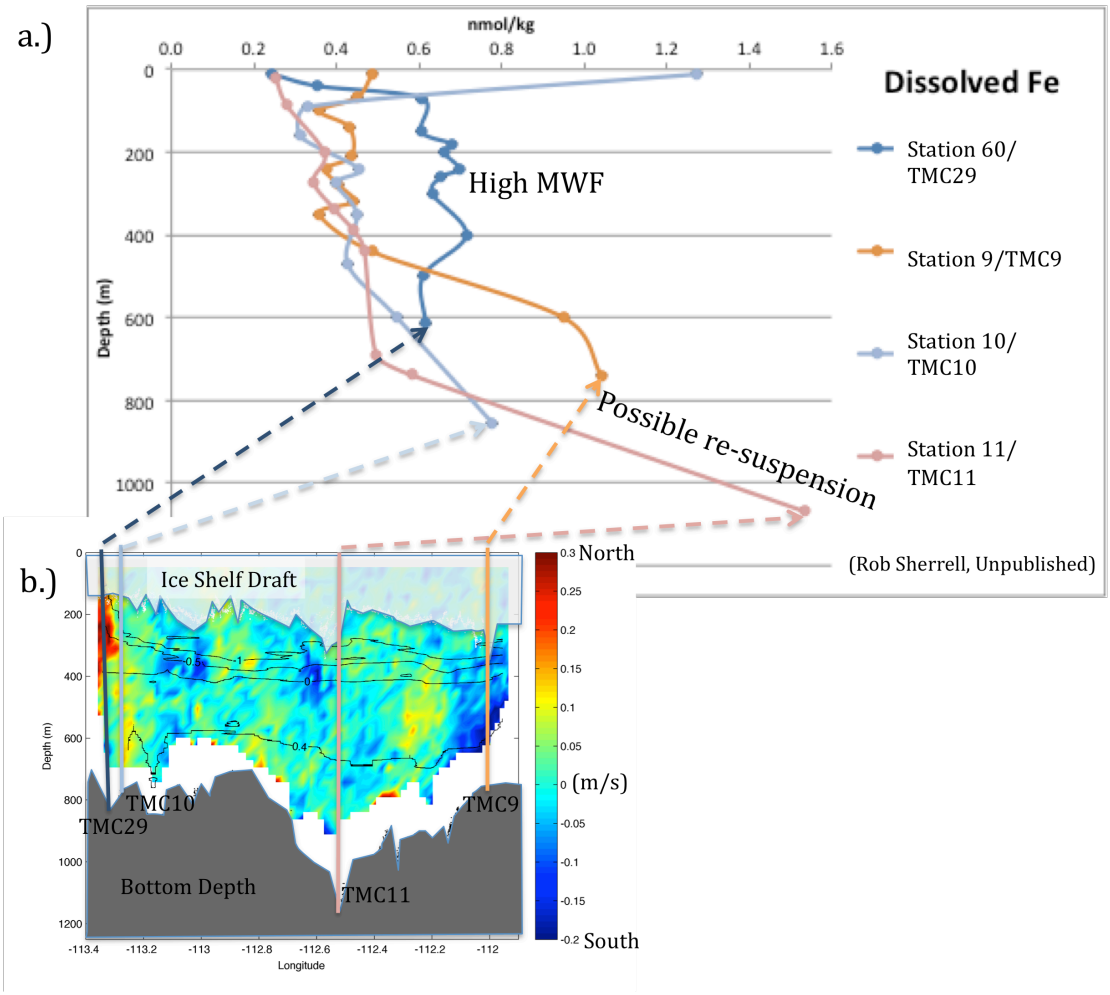

Figure 16: (a) Dissolved (<0.2µm) Fe (dFe) concentrations across the DIS (R. Sherrell, Rutgers University, unpublished). The dFe concentrations near the bottom at most stations are elevated from suspected sedimentary sources. Only the DIS outflow (TM29) has elevated dFe concentrations throughout the water column. (b) Ocean currents from Figure 12 to show locations of TMC casts with respect to enhanced inflow/outflow regions east/west, respectively.

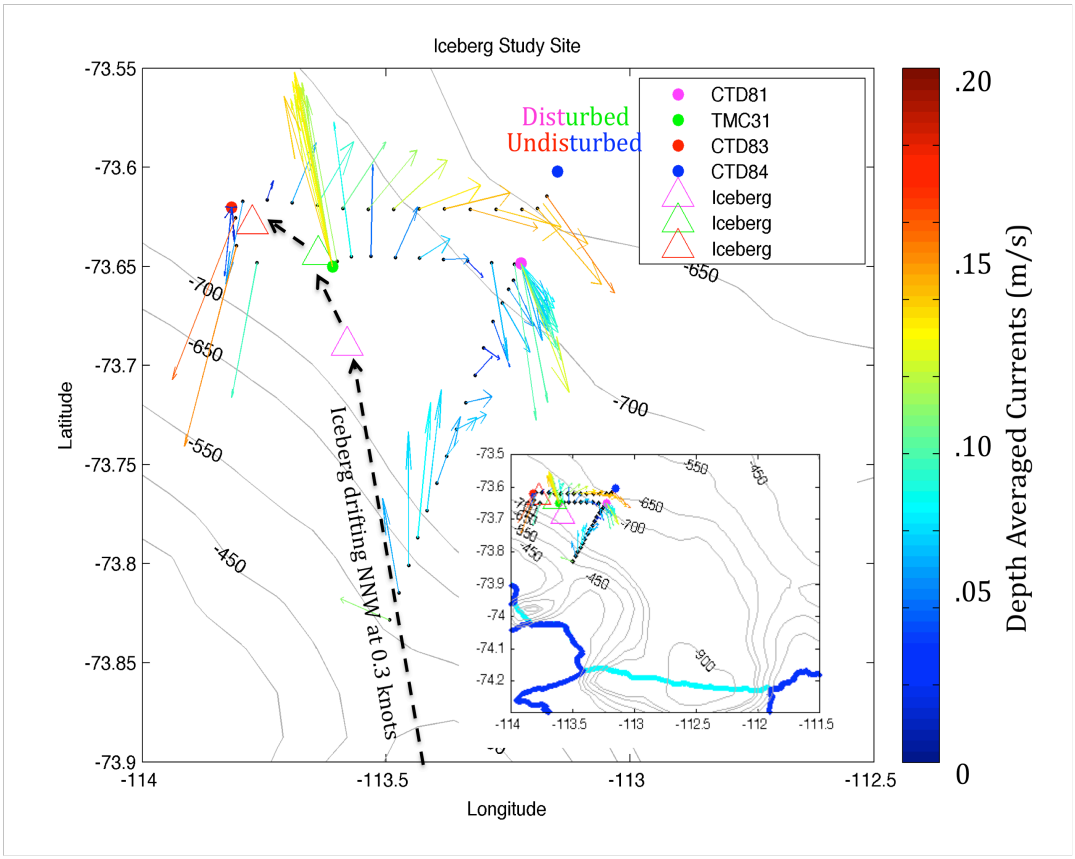

Figure 17: Along-track depth averaged ocean currents for the iceberg study area, showing also locations of the drifting iceberg (triangles) coincident with the 4 CTD casts (indicated by color). CTD casts in the wake of where the iceberg had drifted (labeled Disturbed) showed dynamically mixed properties, while CTD casts in typical polynya waters (labeled Undisturbed) showed homogeneous layers. Iceberg drift trajectory (black dash) and bathymetry (gray contours) are also indicated. (Inset) The iceberg study site was ~ 50 km north of the DIS.

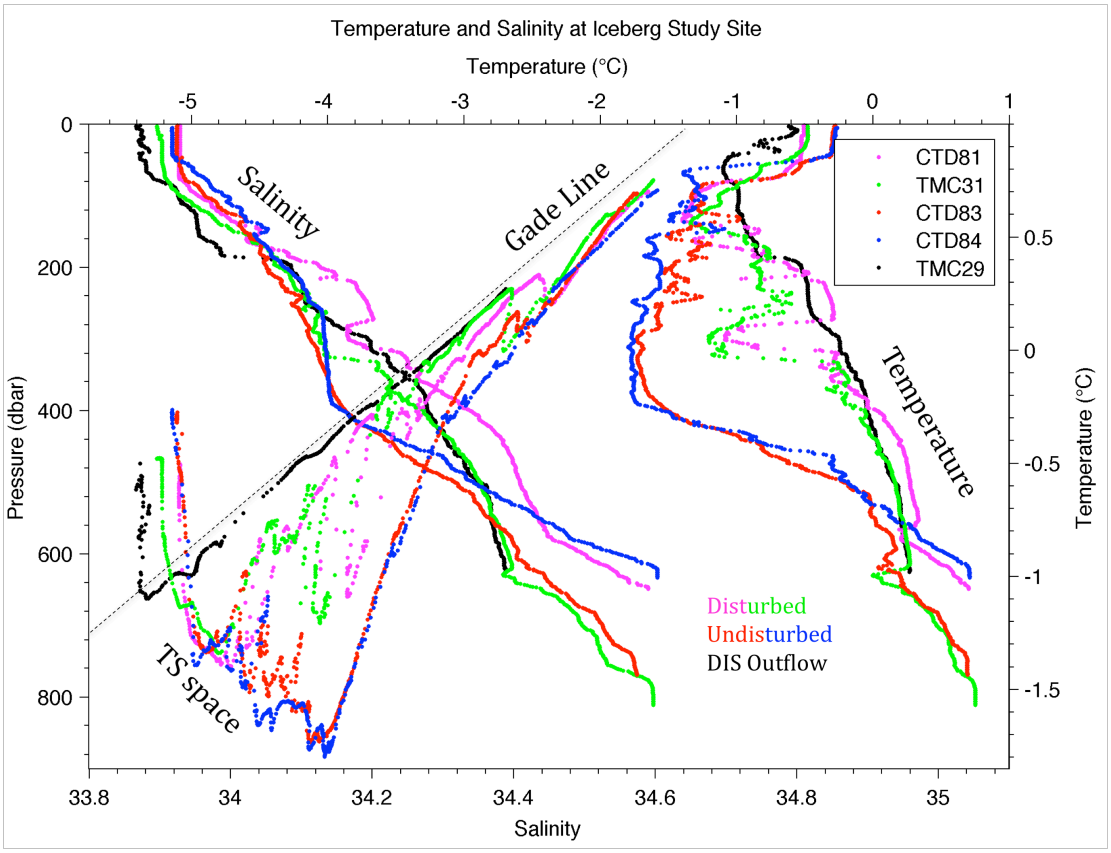

Figure 18: Temperature (T) and salinity (S) data from the 4 CTD casts taken in the iceberg study area, along with the CTD cast from the DIS outflow (TM29). The T/S data are plotted as profiles (left/top/bottom axes) and in T-S space (bottom/right axes). The 'disturbed' CTD casts in the wake of the iceberg were heterogeneously mixed compared to the 'undisturbed' CTD casts, which show more homogeneous water mass layers typical of the ASP. The T/S data from the DIS outflow (TM29) are included for reference to show that the iceberg 'disturbed' CTD casts indicate T-S properties along (at depth) or approaching (at mid-depths) the T/S values of TM29 and the Gade line (black dash). This would indicate some mixing of meltwater at the 'disturbed' CTD cast locations, most of which may likely derive from DIS outflow, but with an unknown amount from in situ melting of the iceberg.

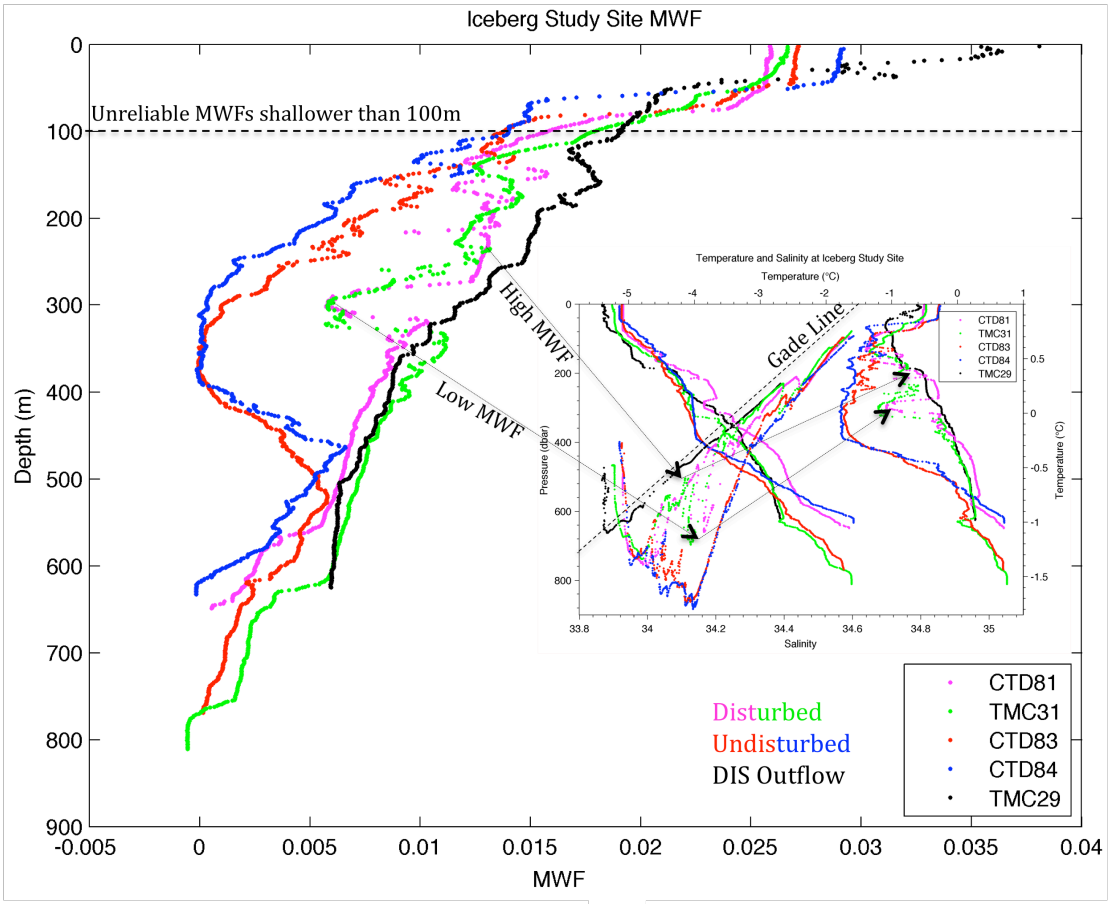

Figure 19: Calculated meltwater fractions (MWF's) from CTD's in the iceberg study area and from the DIS outflow (TM29) for reference. The MWF's from the 'disturbed' CTD cast locations have higher values (approaching the same MWF's as the DIS outflow) than the MWF's from the 'undisturbed' CTD cast locations. Lower MWF's at ~300m coincide with lower dFe concentrations (Figure 20). Meltwater is indistinguishable as to whether it is of iceberg or DIS outflow origin. (Inset) Figure 18 for reference to show T-S features corresponding to high/low MWF's. Surface measurements down to ~100 m are unreliable due to atmospheric influences.

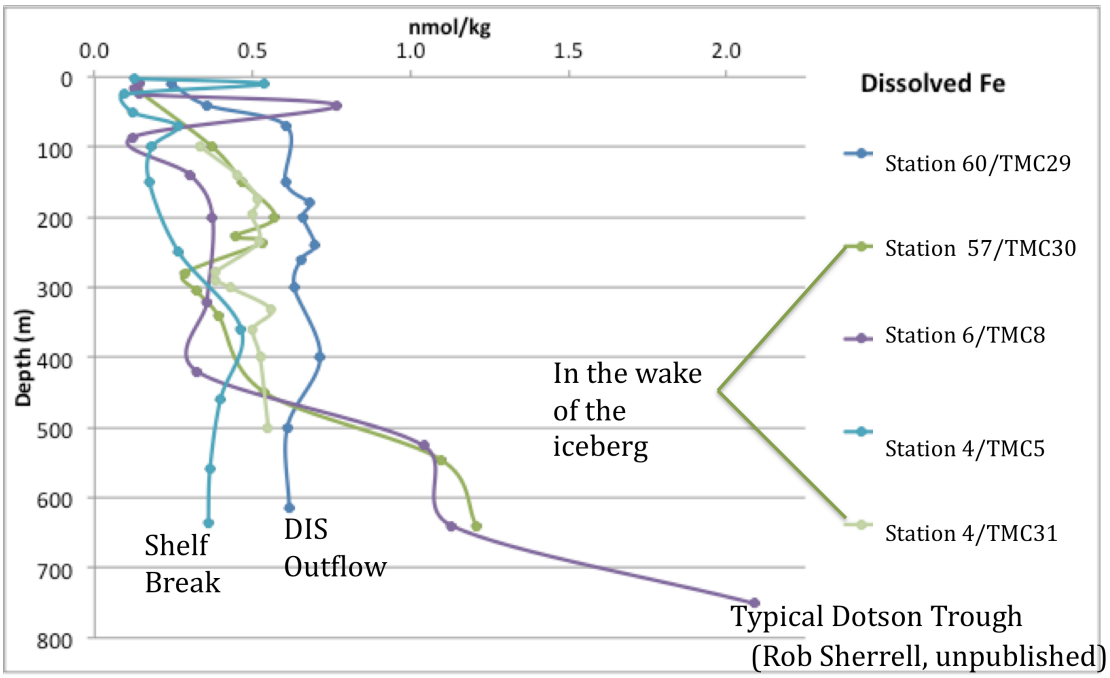

Figure 20: Dissolved (<0.2µm) Fe (dFe) profiles from the iceberg study site (courtesy R. Sherrell, Rutgers University, unpublished) showing dFe concentrations in profiles in the wake of the iceberg (green) that are similar to the DIS outflow. Iceberg mixed and DIS outflow profiles are elevated in dFe compared to typical polynya conditions over the ~80-500m depth interval. High dFe concentrations at >500m depth are likely from sedimentary sources. We note dFe variability corresponds to specific features in the T/S profiles (Figure 18). An unknown quantity of dFe is derived from direct iceberg melting, as opposed to dFe inputs with upwelled melt-laden and mCDW waters.

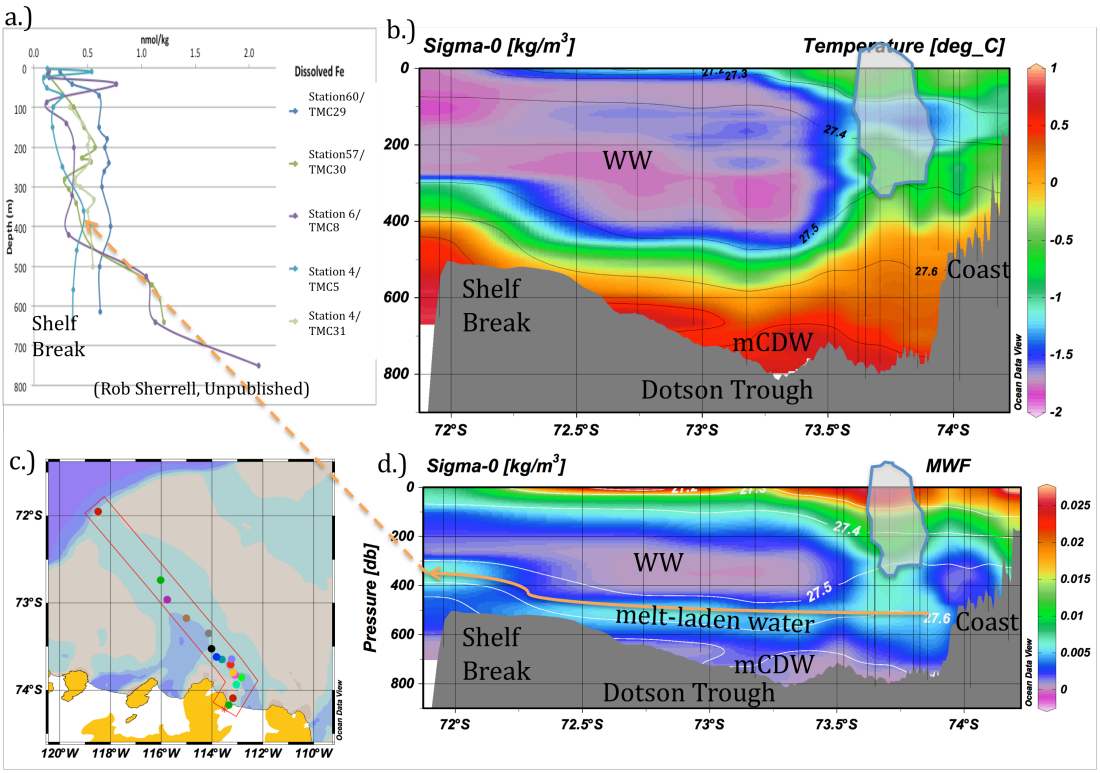

Figure 21: (a); From Figure 20, profiles of dFe concentrations showing for the shelf break station elevated dFe at ~400m, corresponding to a meltwater layer; (b) temperature transect (see (c) for location) with labeled water masses and location of iceberg interaction; (c) map of CTD transect from continental shelf break to DIS outflow; and (d) calculated MWF's along transect in (b, c) showing elevated meltwater concentrations at the ~27.6 isopycnal. Interactions with a drifting iceberg at ~73.75° S appeared to mix melt-laden water to shallower depths compared to other locations along the transect.

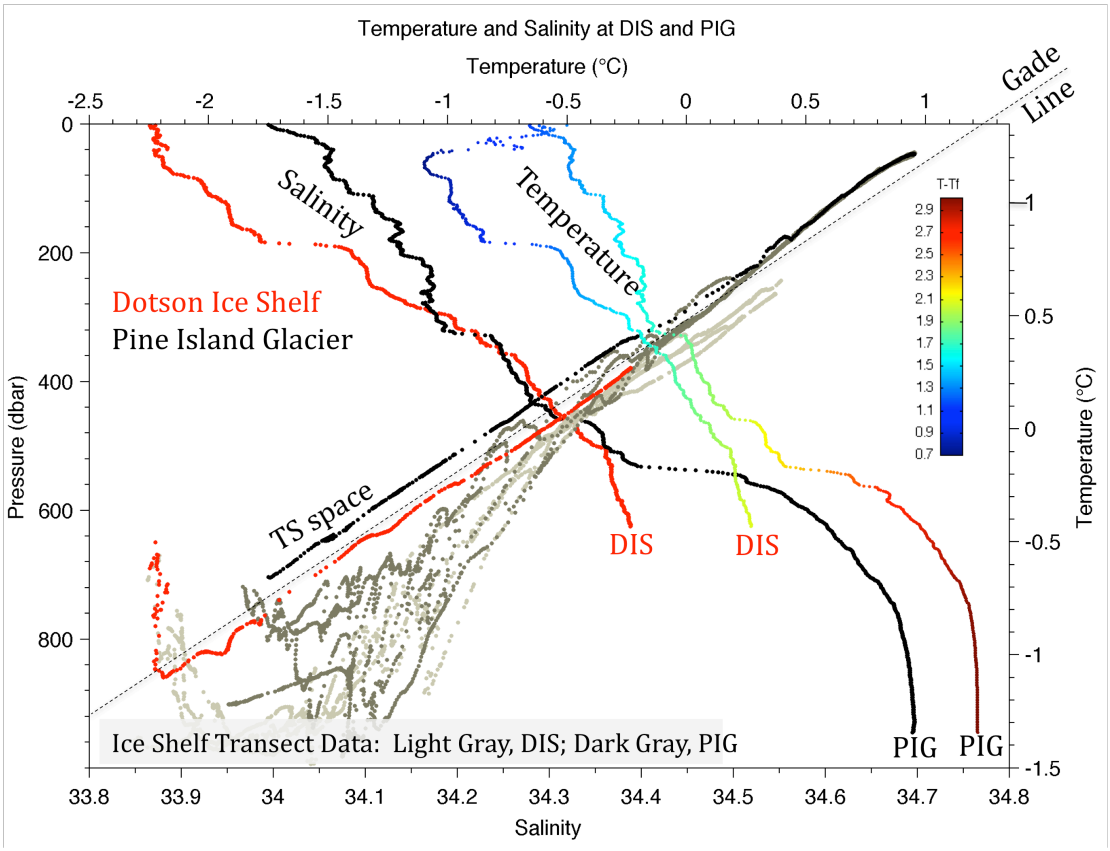

Figure 22: Temperature (T) and salinity (S) data from CTD measurements at Pine Island Glacier (PIG) outflow (black) and DIS outflow (red). The T/S data are plotted as profiles (left/top/bottom axes) and in T-S space (bottom/right axes). The temperature profiles are scaled to degrees (°C) above freezing (T – Tf). Other CTDs across PIG (dark gray) and DIS (light gray) appear in T-S space. The Gade line (black dash) is overlaid in T-S space and only the PIG and DIS outflow fall close to the calculated mixing line between meltwater and mCDW. The mCDW in front of PIG is distinctly warmer and saltier than mCDW in front of DIS. The PIG data are from Jacobs et al. (2011).

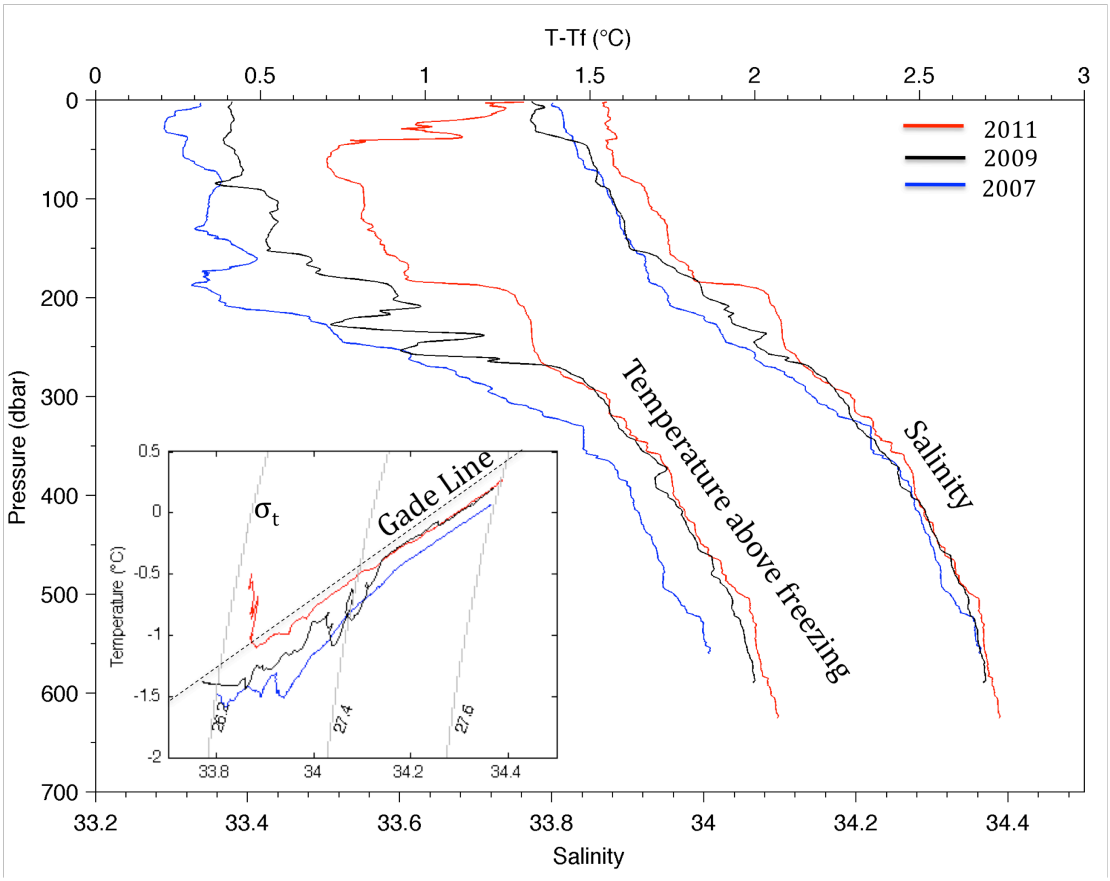

Figure 23: Profiles of temperature above freezing and salinity at the DIS outflow from 2007, 2009 and 2011. All profiles were taken within 0.5 km of each other. There have been warmer conditions at the DIS outflow since 2007. (Inset) The same data plotted in T-S space and overlaid with the Gade line (black dash). The 2011 DIS outflow data appear closer to the Gade line throughout most of the water column, indicating an overall higher amount of meltwater. Isopycnals (gray contours) are sigma-t.

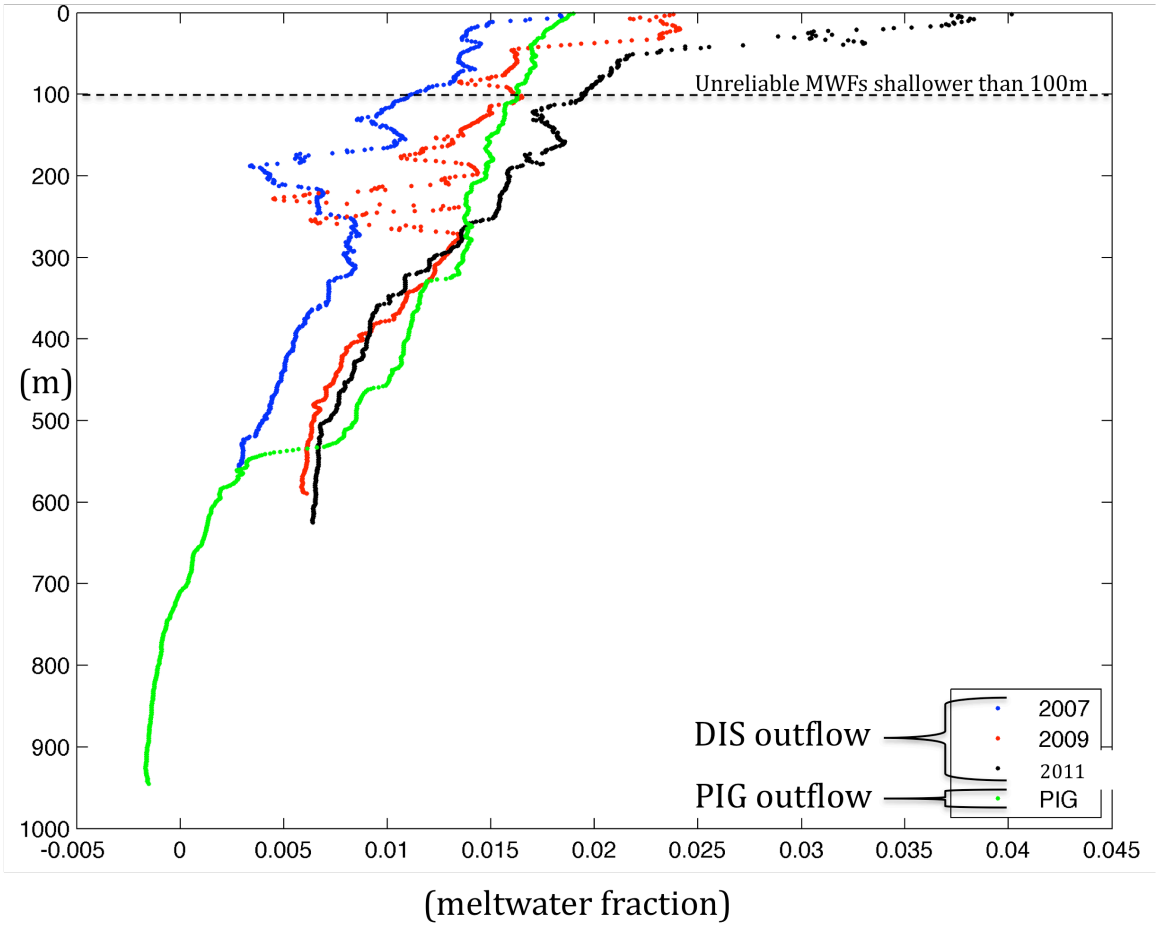

Figure 24: Calculated meltwater fractions (MWF's) at the DIS outflow (labeled by year) and PIG outflow. The mCDW entering the PIG is warmer than DIS, yet calculated meltwater fractions are similar. Surface measurements down to ~100 m are unreliable due to atmospheric influences.

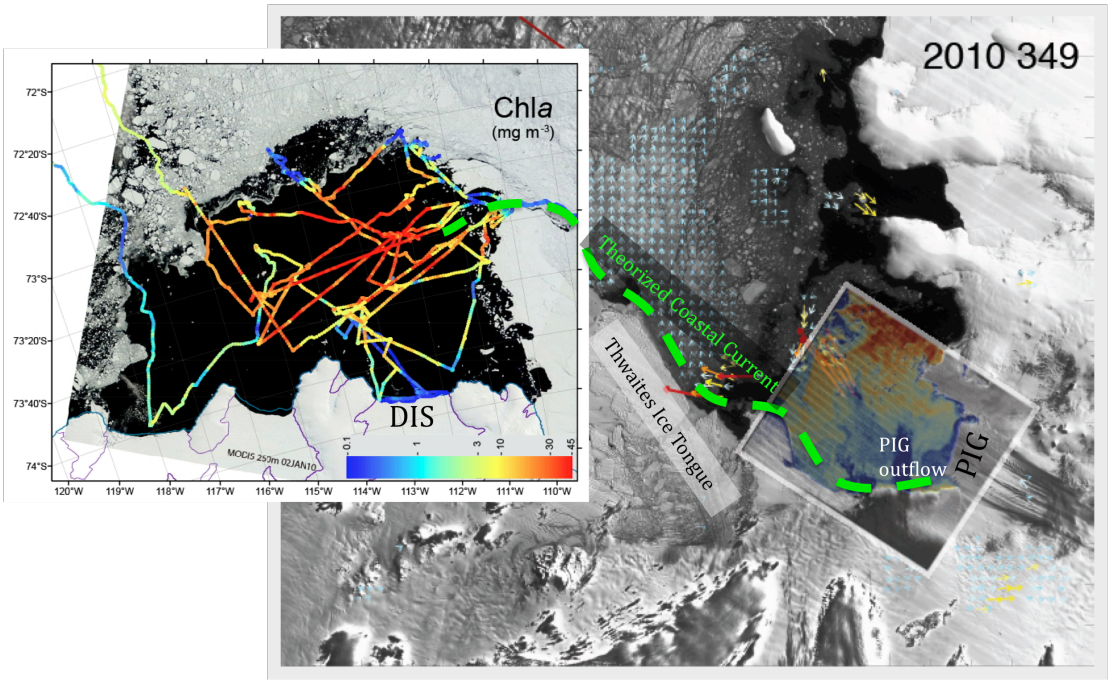

Figure 25: Overlapped satellite images to show inferred coastal current of meltwater outflow (green dash) originating from PIG and reaching the eastern ASP. The background image of the eastern Amundsen Sea was created by Ken Mankoff (unpublished) and includes a MODIS image from Dec 15, 2010, overlaid with (i) derived ice velocity vectors (colored arrows), and (ii) a thermal infrared Landsat image of Pine Island Bay showing sea surface temperature. The ASP image overlaid on the left is from Figure 1 (created by Povl Abrahamsen) and is geo-located to the underlying image mosaic to show the hypothesized coastal current extending into the ASP region. If such a current exists, it would be highly enriched with dFe from e.g., PIG meltwater outflow, melting sea ice and iceberg meltwater and could therefore fuel potentially large phytoplankton blooms in the ASP.

Tables

Location	Cruise	CTD	Z_{WW}	T_{WW}	T_{CDW}	Z_{CDW}	S_{WW}	S_{CDW}
PIG	NBP0901	CTD23	312	-1.38	1.15	707	34.10	34.66
DIS	NBP1005	TMC11	215	-1.40	0.66	1067	34.0	34.55
Iceberg	NBP1005	CTD84	383	-1.754	0.075	630	34.14	34.60

Table 1: Values used to calculate MWF's at each location. The $Z_{WW,CDW}$ are the depths selected for extracting the WW and CDW temperature and salinity values. The $T_{WW,CDW}$ are the temperatures of CDW and WW, and $S_{WW,CDW}$ are the salinities of CDW and WW.

Water Mass	Temperature (°C)	Salinity (psu)	Oxygen (ml/L)	dFe (nM)	Density (sigma-t)	Depth (m)
CDW	1.7	34.7	<5	>2.8	27.8	PIG only
mCDW	0.7	34.5	<5	1 to 2	27.6	>700
Melt-laden layer	-1.0 to 0.25	34.1 to 34.3	5 to 6	~1	27.5 to 27.3	200 to 600
WW	-1.8 to -1.4	33.8 to 34.1	>6	<0.5	27.4	200 to 300
AASW	-1.8 to 0.5	33.5 to 34.0	~9	<0.1	<27.3	<100

Table 2: Typical Water Masses found in the Amundsen Sea (based on: Wåhlin et al., 2010; Orsi et al., 1995; Jacobs et al., 2011; Löscher et al., 1997; Sherrell (unpublished iron data), and NBP1005 data).

Station	Date	Latitude	Longitude	In Wake	Km from Iceberg
CTD81	1/2/11 18:09	-73 .65	-113.22	Yes	10
TMC31	1/3/11 05:42	-73.65	-113.61	Yes	0.5
CTD83	1/3/11 12:15	-73.62	-113 .82	No	1
CTD84	1/3/11 17:21	-73.60	-113.149	No	15

Table 3: CTDs within the iceberg study site. The CTD81 and TMC31 casts were in heterogeneously mixed waters while the CTD 83 and CTD84 casts were in more typical polynya waters.

Water Mass	Temperature (°C)	Salinity (psu)	Depth (m)
ASP mCDW	0.75	34.7	>750
ASP WW	-1.60	34.08	300
Weddell mCDW	0.40	34.65	300
Weddell WW	-1.50	34.47	150

Table 4: Typical water mass characteristics in the Amundsen Sea versus the Weddell Sea.

Appendix

List of Acronyms

ACC……Antarctic Circumpolar Current

ADCP……Acoustic Doppler Current Profiler

ASL……Amundsen Sea Low

ASP……Amundsen Sea Polynya

ASPIRE……Amundsen Sea Polynya International Research Expedition

CDW……Circumpolar Deep Water

CTD……Conductivity Temperature Depth

DIS……Dotson Ice Shelf

ENSO……El Nino Southern Oscillation

LCDW……Lower Circumpolar Deep Water

mCDW……Modified Circumpolar Deep Water

MWF……Melt Water Fraction

nb150……narrow beam 150 kHz ADCP

NBP……Nathaniel B Palmer

NBP0702……Nathaniel B Palmer (2007 cruise)

NBP0901……Nathaniel B Palmer (2009 cruise)

NBP1005……Nathaniel B Palmer (2010 cruise)

os38……ocean surveyor 38 kHz ADCP

PIG……Pine Island Glacier

SAM……Southern Annular Mode

SSS……Sea Surface Salinity

SST……Sea Surface Temperature

TMC……Trace Metal Clean CTD

TS……Temperature-Salinity space

UCDW……Upper Circumpolar Deep Water

WAIS……Western Antarctic Ice Sheet

wAP……western Antarctic Peninsula

WW……Winter Water

XBT……Expendable Bathythermograph

Bibliography

Alderkamp, A. C., Mills, M. M., van Dijken, G. L., Laan, P., Thuróczy, C.E., Gerringa, L. J. A., de Baar, H. J. W., et al. (2012). Iron from melting glaciers fuels phytoplankton blooms in the Amundsen Sea (Southern Ocean): Phytoplankton characteristics and productivity. *Deep Sea Research Part II: Topical Studies in Oceanography*. doi:10.1016/j.dsr2.2012.03.005 (in press).

Arrigo, K.R., Worthen, D., Schnell, A., Lizotte, M. P. (1998). Primary production in Southern Ocean waters. *Journal of Geophysical Research*, *103*(C8), 15587–15. American Geophysical Union.

Arrigo, Kevin R. (2003). Phytoplankton dynamics within 37 Antarctic coastal polynya systems. *Journal of Geophysical Research*, *108*(C8). doi:10.1029/2002JC001739.

Arrigo, K. R., Lowry, K. E., & van Dijken, G. (2012). Annual changes in sea ice and phytoplankton in polynyas of the Amundsen Sea, Antarctica. *Deep Sea Research Part II: Topical Studies in Oceanography*. Elsevier. doi:10.1016/j.dsr2.2012.03.006.

Boyd, P. W., Watson, a J., Law, C. S., Abraham, E. R., Trull, T., Murdoch, R., Bakker, D. C., et al. (2000). A mesoscale phytoplankton bloom in the polar Southern Ocean stimulated by iron fertilization. *Nature*, *407*(6805), 695-702. doi:10.1038/35037500.

Comiso, J. C., F. Nishio (2008), Trends in the sea ice cover using enhanced and compatible AMSR-E, SSM/I, and SMMR data, *J. Geophys. Res.*, 113, C02S07, doi:10.1029/2007JC004257.

Conway, H. (1999). Past and Future Grounding-Line Retreat of the West Antarctic Ice Sheet. *Science*, *286*(5438), 280-283. doi:10.1126/science.286.5438.280.

De Baar, H. J. W., de Jong, J. T. M., Bakker, D. C. E., Löscher, B. M., Veth, C., Bathmann, U., Smetacek, V. (1995). Importance of iron for plankton blooms and carbon dioxide drawdown in the southern ocean. Nature Publishing Group.

Dierssen, H. M., Smith, R. C., Vernet, M. (2002). Glacial meltwater dynamics in coastal waters west of the Antarctic peninsula. *Proceedings of the National Academy of Sciences of the United States of America*, *99*(4), 1790-5. doi:10.1073/pnas.032206999.

Ding, Q., E.J. Steig, D.S. Battisti and M. Küttel. 2011. Winter warming in West Antarctica caused by central tropical Pacific warming. *Nature Geosci.,* **4**(6), 398–403.

Gade, H.G. (1979). Melting of Ice in Sea Water: A Primitive Model with Application to the Antarctic Ice Shelf and Icebergs. *Journal of Physical Oceanography*, 189-198.

Hiscock, M., Marra, J., Smith, W., Goericke, R., Measures, C., Vink, S., Olson, R., et al. (2003). Primary productivity and its regulation in the Pacific Sector of the Southern Ocean. *Deep Sea Research Part II: Topical Studies in Oceanography*, *50*(3-4), 533-558. doi:10.1016/S0967-0645(02)00583-0.

Jacobs, S. S., Hellmer, H. H., Jenkins, A. (1996). Antarctic ice sheet melting in the Southeast Pacific. *Geophysical Research Letters*, *23*(9), 957–960. American Geophysical Union.

Jacobs, S. S., Giulivi, C., Mele, P. (2002). Freshening of the Ross Sea during the late 20th century. *Science*, *297*(5580), 386. American Association for the Advancement of Science. doi:10.1126/science.1069574.

Jacobs, S. (2006). Observations of change in the Southern Ocean. *Philosophical transactions. Series A, Mathematical, physical, and engineering sciences*, *364*(1844), 1657-81. doi:10.1098/rsta.2006.1794.

Jacobs, S. S., Jenkins, A., Giulivi, C. F., Dutrieux, P. (2011). Stronger ocean circulation and increased melting under Pine Island Glacier ice shelf. *Nature Geoscience*, *4*(8), 519-523. Nature Publishing Group. doi:10.1038/ngeo1188.

Jenkins, Adrian. (1999). The Impact of Melting Ice on Ocean Waters. *Journal of Physical Oceanography*, *29*(9), 2370-2381. doi:10.1175/1520-0485(1999)029<2370:TIOMIO>2.0.CO;2.

Jenkins, Adrian, Jacobs, S. (2008). Circulation and melting beneath George VI Ice Shelf, Antarctica. *Journal of Geophysical Research*, *113*(C4), 1-18. doi:10.1029/2007JC004449.

Jenkins, A., Dutrieux, P., Jacobs, S. S., McPhail, S. D., Perrett, J. R., Webb, A. T., White, D. (2010). Observations beneath Pine Island Glacier in West Antarctica and implications for its retreat. *Nature Geoscience*, *3*(7), 468-472. Nature Publishing Group. doi:10.1038/ngeo890.

Lucchitta, B. K., Mullins, K. F., Smith, C. E., Ferrigno, J. G. (1994). Velocities of the Smith Glacier ice tongue and Dotson Ice Shelf, Walgreen Coast, Marie Byrd Land, West Antarctica. *Annals Of Glaciology*, *20*, 101-109.

Mankoff, K. D., Jacobs, S. S., Tulaczyk, S. M., Stammerjohn, S. E. (2012). The role of Pine Island Glacier ice shelf basal channels in deep-water upwelling, polynyas and ocean circulation in Pine Island Bay, Antarctica. *Annals of Glaciology*, *53*(60), 123-128. doi:10.3189/2012AoG60A062.

Marshall, G.J. (2003). Trends in the southern annular mode from observations and reanalyses. *J. Climate*, 16(24), 4134-4143.

Martinson, D. G. (2011). Transport of warm upper circumpolar deep water onto the Western Antarctic Peninsula Continental Shelf. *Ocean Science*, *8*(1), 1-24. doi:10.5194/osd-8-1-2011. (Accepted).

Montes-Hugo, M., Doney, S., Ducklow, H. W., Fraser, W., Martinson, D., Stammerjohn, S. E., Schofield, O. (2009). Recent Changes in Phytoplankton Communities Associated with Rapid Regional Climate Change Along the Western Antarctic Peninsula. *Science*, *323*(5920), 1470. American Association for the Advancement of Science.

Neshyba, S. (1977). Upwelling by icebergs. *Nature*, *267*, 507-508. Nature Publishing Group.

Nitsche, F. O., Jacobs, S. S., Larter, R. D., Gohl, K. (2007). Bathymetry of the Amundsen Sea continental shelf: Implications for geology, oceanography, and glaciology. *Geochemistry Geophysics Geosystems*, *8*(10), 1-10. doi:10.1029/2007GC001694.

Orsi, A.H., Whitworth, T., Nowlin, W. D., et al. (1995). On the meridional extent and fronts of the Antarctic Circumpolar Current. *Deep Sea Research Part I: Oceanographic Research Papers*, *42*(5), 641–673. Elsevier.

Orsi, Alejandro H., Wiederwohl, C. L. (2009). A recount of Ross Sea waters. *Deep Sea Research Part II: Topical Studies in Oceanography*, *56*(13-14), 778-795. Elsevier. doi:10.1016/j.dsr2.2008.10.033

Planquette, H., Sherrell, R. M., Stammerjohn, S., Field, M. P. (2011). Mechanisms of particulate iron delivery to the water column of the Amundsen Sea, Antarctica. *Global Biogeochemical Cycles*, (Submitted).

Potter, J. R., Talbot, M. H., Paren, J. G. (1988). Oceanic regimes at the ice fronts of George VI Sound, Antarctic Peninsula. *Continental Shelf Research*, *8*(4), 347–362. Elsevier.

Rignot, E. J. (1998). Fast Recession of a West Antarctic Glacier. *Science*, *281*(5376), 549-551. doi:10.1126/science.281.5376.549.

Rignot, E., Bamber, J. L., van den Broeke, M. R., Davis, C., Li, Y., van de Berg, W. J., van Meijgaard, E. (2008). Recent Antarctic ice mass loss from radar interferometry and regional climate modelling. *Nature Geoscience*, *1*(2), 106-110. doi:10.1038/ngeo102.

Rosanova, C. E., Lucchitta, B. K., Ferrigno, J. (1998). Velocities of Thwaites Glacier and stnaller glaciers along the Marie Byrd Land coast, West Antarctica. *Annals Of Glaciology*, *27*, 47-53.

Sarmiento, J., Toggweiler, J. (1984). A new model for the role of the oceans in determining atmospheric pCO 2. *Nature*, *308*(5960), 621–624.

Schneider, D.P., C. Deser, Y. Okumura. (2012). An assessment and interpretation of the observed warming of West Antarctica in the austral spring. *Clim. Dyn.*, doi: 10.1007/s00382-010-0985-x.

Schwarz, J. N., Schodlok, M. P. (2009). Impact of drifting icebergs on surface phytoplankton biomass in the Southern Ocean: Ocean colour remote sensing and in situ iceberg tracking. *Deep Sea Research Part I: Oceanographic Research Papers*, *56*(10), 1727-1741. doi:10.1016/j.dsr.2009.05.003.

Sedwick, P. N., Marsay, C. M., Sohst, B. M., Aguilar-Islas, A. M., Lohan, M. C., Long, M. C., Arrigo, K. R., et al. (2011). Early season depletion of dissolved iron in the Ross Sea polynya: Implications for iron dynamics on the Antarctic continental shelf. *Journal of Geophysical Research*, *116*(C12), 1-19. doi:10.1029/2010JC006553.

Shepherd, A, Wingham, D. J., Mansley, J. A, Corr, H. F. (2001). Inland thinning of Pine Island Glacier, West Antarctica. *Science (New York, N.Y.)*, *291*(5505), 862-4. doi:10.1126/science.291.5505.862.

Shepherd, A. (2004). Warm ocean is eroding West Antarctic Ice Sheet. *Geophysical Research Letters*, *31*(23), 4-7. doi:10.1029/2004GL021106.

Smith, K. L., Robison, B. H., Helly, J. J., Kaufmann, R. S., Ruhl, H. A, Shaw, T. J., Twining, B. S., et al. (2007). Free-drifting icebergs: hot spots of chemical and biological enrichment in the Weddell Sea. *Science (New York, N.Y.)*, *317*(5837), 478-82. doi:10.1126/science.1142834.

Smith, W. O., Nelson, D. M. (1985). Phytoplankton Bloom Produced by a Receding Ice Edge in the Ross Sea: Spatial Coherence with the Density Field. *Science* (New York, NY), 227(4683), 163-166. *DOI:10.1126/science.227.4683.163.*

Stammerjohn, S. E., Massom, R. A., Rind, D., Martinson, D. G. (2012), Regions of rapid sea ice change: an inter-hemispheric seasonal comparison, *Geophysical Research Letters, 39* (L06501), doi: 10.1029/2012GL050874.

Stammerjohn, S. E., Martinson, D. G., Smith, R. C., Yuan, X., Rind, D. (2008). Trends in Antarctic annual sea ice retreat and advance and their relation to El Niño–Southern Oscillation and Southern Annular Mode variability. *Journal of Geophysical Research*, *113*(C3), 1-20. doi:10.1029/2007JC004269

Steig, E. J., Ding, Q., Battisti, D. S., Jenkins, A. (2012). Tropical forcing of Circumpolar Deep Water Inflow and outlet glacier thinning in the Amundsen Sea Embayment , West Antarctica. *Annals Of Glaciology*, (53), 19-28. doi:10.3189/2012AoG60A110.

Stephenson Jr., G. R., Sprintall, J., Gille, S. T., Vernet, M., Helly, J. J., Kaufmann, R. S. (2010). Subsurface melting of a free-floating Antarctic iceberg. *Deep Sea Research Part II: Topical Studies in Oceanography*, 1-10. Elsevier. doi:10.1016/j.dsr2.2010.11.009.

Thoma, M., Jenkins, A., Holland, D., Jacobs, S. (2008). Modelling Circumpolar Deep Water intrusions on the Amundsen Sea continental shelf, Antarctica. *Geophysical Research Letters*, *35*(18), 1-6. doi:10.1029/2008GL034939.

Turner, J., Bindschadler, R., Convey, P., et al. (2009). Antarctic climate change and the environment. *SCAR & Scott Polar Research Institute, Cambridge,* (1), ISBN 978-0-948277-22-1.

Walker, D. P., Brandon, M. A., Jenkins, A., Allen, J. T., Dowdeswell, J. A., Evans, J. (2007). Oceanic heat transport onto the Amundsen Sea shelf through a submarine glacial trough. *Geophysical Research Letters*, *34*(2). doi:10.1029/2006GL028154.

Wåhlin, A. K., Yuan, X., Björk, G., Nohr, C. (2010). Inflow of Warm Circumpolar Deep Water in the Central Amundsen Shelf. *Journal of Physical Oceanography*, *40*(6), 1427-1434. doi:10.1175/2010JPO4431.1.

Wåhlin, A. K., Muench, R. D., Arneborg, L., Björk, G., Ha, H. K., Lee, S. H., Alsén, H. (2012). Some Implications of Ekman Layer Dynamics for Cross Shelf Exchange in the Amundsen Sea. *Journal of Physical Oceanography*, 120308135555000. doi:10.1175/JPO-D-11-041.1 (accepted).

Yuan, X., Sambrotto, R., Stammerjohn, S., Smethie Jr., W. M., Bjork, G., Wahlin, A. K., Li, C. (2012). Spatial Variability of Water Masses on the Amundsen Sea Shelf. (submitted).